PHYSICAL REVIEW D VOLUME 19, NUMBER 8 15 APRIL 1979

Scale breaking for quark and gluon distributions in quantum chromodynamics: A diagrammatic analysis

William R. Frazer
Department of Physics, B-019, University of California, San Diego, La Jolla, California 92093

John F. Gunion
Department of Physics, University of California, Davis, California 95616
(Received 5 October 1978)

We demonstrate that, in an appropriately chosen axial gauge, the leading contributions to the scale breaking of quark and gluon distributions in quantum chromodynamics arise from fully renormalized ladder graphs. These may be conveniently summed using the Bethe-Salpeter equation and reproduce the standard results obtained via the operator-product-expansion–renormalization-group analysis. The diagrammatic analysis makes it clear that scale breaking (from the two-particle reducible ladder graphs) of the distributions is universal and factorizes, in any parton-model application, from the short-distance (two-particle irreducible) "subprocess." In addition, the dominance of ladder diagrams can be used to justify the Altarelli-Parisi approach to scale breaking including a demonstration that their infrared regularization scheme arises naturally when quark and gluon wave-function renormalization is properly included.

I. INTRODUCTION

Despite the beauty of the operator-product–renormalization-group approach to the analysis of scale breaking for deep-inelastic scattering in quantum chromodynamics (QCD), an intuitive (Feynman) diagrammatic understanding has been lacking. This has led to some uncertainity as to how to extend this type of analysis to reactions other than deep-inelastic scattering.

In this paper we demonstrate, by extending a method developed by Appelquist and Poggio[1] in $(\phi^3)_6$ theory that a simple diagrammatic understanding of scale breaking in QCD is possible. Instead of the renormalization-group equations we use the Bethe-Salpeter equation and work in the leading-logarithm approximation. The operator-product expansion is replaced by the more pedestrian partial-wave expansion of the Bethe-Salpeter equation. If one chooses an appropriate axial gauge, then only renormalized ladder graphs contribute and the scale-breaking diagrams are easily summed. The axial-gauge ladder structure makes it clear that the scale-breaking structure and related singularities in the hadron masses are entirely associated with the two-particle reducible ladder sum and factorize from the two-particle irreducible short-distance "subprocess" ($q\gamma^* \to \gamma^* q$ in the case of deep-inelastic scattering). This implies that any parton-model calculation is modified by the scale-breaking effects of QCD in the most straightforward manner: One simply employs universal scale-broken quark/gluon distribution functions (as determined in the axial gauge by the two-particle reducible ladder sums—one for each interacting quark or gluon). In the axial gauge one computes the two-particle irreducible part of the short-distance subprocess (which is infrared finite) to a desired order in $\alpha_s(\text{"}Q^2\text{"})$, the moving coupling constant evaluated at an appropriate momentum transfer squared, and folds this together with the scale-broken distribution functions of the colliding objects. To leading order in $\alpha_s(\text{"}Q^2\text{"})$ the short-distance subprocess is always an elementary "Born" graph, e.g., $q\gamma^* \to \gamma^* q$ for deep-inelastic scattering, $q\bar{q} \to \mu^+\mu^-$ for μ pair production, $q_1 q_2 \to q_1 q_2$ for high-p_T jet production, etc.

We perform explicit calculations for deep-inelastic lepton scattering off quarks. We demonstrate that the straightforward solution of the Bethe-Salpeter ladder equation in the axial gauge reproduces the standard anomalous-dimension results for W_1. The calculation of the longitudinal structure function W_L, which vanishes in the leading-log approximation, introduces the additional complication of nonleading contributions. One finds that the dominant contribution in such a case occurs when the nonleading effects are confined to a single loop integral, the one at the top of the ladder nearest the hard photons.

In Sec. II we first exhibit the diagrammatic method and its implications for general short-distance parton-model applications in a model field theory, ϕ^3 theory in six dimensions. In Sec. III the method is extended to QCD, illustrating its application to deep-inelastic scattering of leptons off quarks. In Sec. IV we show how this diagrammatic technique can be used to derive the Altarelli-Parisi[2] scheme for scale-breaking calculations. In particular, the dominance of ladder diagrams justifies their intuitive brems-

strahlung model and their scheme for regularizing the infinities in the moments of the bremsstrahlung distributions emerges as a natural result of properly including quark and gluon wave-function renormalizations. Section V summarizes our results and their implications.

In a second paper we will demonstrate how this diagrammatic method may be used to provide a simple analysis of deep-inelastic scattering of leptons off nearly real photons and of jet production in photon-photon collisions. Because of the elementary nature of the photon, it turns out that processes such as $\gamma\gamma \to q\bar{q}$ via quark exchange exhibit naive scaling.

II. DEEP-INELASTIC SCATTERING IN ϕ^3 THEORY IN SIX DIMENSIONS

Appelquist and Poggio[1] have shown how to use the Bethe-Salpeter equation to analyze deep-inelastic scattering in ϕ^3 field theory in six dimensions, $(\phi^3)_6$. In this section we review and extend their method, remaining within the context of the model. We shall thus be able to discuss some general features of the method, free from the spin and gauge complications of QCD. These latter complications will be treated in Sec. III.

We shall be concerned with the behavior of the two-particle scattering amplitude $M(p,q)$, where the momenta are defined in Fig. 1, in the limit

$$q^2 \to \infty, \quad p^2/q^2 \to 0, \quad \omega \equiv 2p\cdot q/q^2 \to 0. \tag{2.1}$$

Throughout, we take all momenta to be Euclidean, and continue back to Minkowski space only at the end of the calculation. Since the limit defined above is not the one appropriate to deep-inelastic scattering, we shall have to continue to the physical region $\omega > 1$ by means of the usual moment expansion.

Appelquist and Poggio showed that the Bethe-Salpeter equation can be used to analyze the behavior of $M(p,q)$ in the limit (2.1). They observed that if $K(p,q)$ is the two-particle irreducible amplitude, then $K(p,q)$ is free from infrared singularities as $p \to 0$. The limit (2.1) can then be taken for $K(p,q)$ as a simple short-distance limit, and $K(p,q)$ is given simply by the one-particle exchange graph in Fig. 2,

$$K(p,q) \sim \frac{1}{q^2}\left[\ln\left(\frac{q^2}{\lambda^2}\right)\right]^{-1-2\gamma}. \tag{2.2}$$

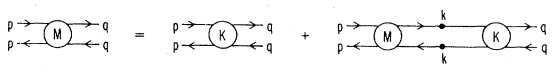

FIG. 1. The Bethe-Salpeter equation obeyed by the two-particle scattering amplitude, M. K is the two-particle irreducible (2PI) kernel.

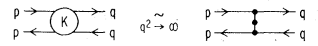

FIG. 2. The short-distance limit of the 2PI kernel. The vertex blobs represent the 1PI vertex corrections. The blob on the propagator represents the full propagator correction with the asymptotic behavior displayed in Eq. (2.3).

The anomalous dimension γ is associated with the asymptotic form of the full propagator,

$$D(q^2) \sim \frac{1}{q^2}\left[\ln\left(\frac{q^2}{\lambda^2}\right)\right]^{\gamma}. \tag{2.3}$$

To understand the behavior (2.2) we first recall that the square of the fully renormalized vertex behaves as[3]

$$\bar{g}^2(q^2/\lambda^2) \equiv 4\pi\,\alpha_s(q^2/\lambda^2) \sim \frac{1}{b\,\ln(q^2/\lambda^2)} \tag{2.4}$$

when evaluated at a symmetric Euclidean point. A renormalized vertex consists of the one-particle irreducible (1PI) vertex and *half* a propagator renormalization for each of the three lines. Hence the square, $\bar{g}^2(q^2/\lambda^2)$, contains a factor $[\ln(q^2/\lambda^2)]^{3\gamma}$ from the propagator renormalizations. The square of the amputated 1PI strong vertex thus behaves as $[b\,\ln(q^2/\lambda^2)]^{-1-3\gamma}$. Since the 1PI vertex is infrared finite this behavior is characteristic [up to corrections of higher order in $\bar{g}^2(q^2/\lambda^2)$] of the squared 1PI vertex evaluated in the asymmetric momentum configuration $(p, q, p-q;\ p^2 \approx 0,\ q^2 \to \infty)$ appropriate to the Bethe-Salpeter equation, Fig. 2. The kernel of Fig. 2 consists of the asymmetrically evaluated 1PI vertex squared and one fully renormalized propagator behaving in the limit (2.1) as $q^{-2}[\ln(q^2/\lambda^2)]^{\gamma}$, which yields finally

$$K(p,q) \sim \frac{1}{b[\,\ln(q^2/\lambda^2)]^{1+3\gamma}}\ \frac{1}{q^2}\,[\ln(q^2/\lambda^2)]^{\gamma},$$

which is just Eq. (2.2). Corrections to this asymptotic form are of relative order $[\ln(q^2/\lambda^2)]^{-1}$, and arise both from the asymmetric momentum configuration and from higher-order kernels.

Note that we have taken the relation (2.4) for the running coupling constant as a fundamental assumption of our analysis. In the following, we scale all momenta such that $\lambda = 1$.

Instead of proving the infrared finitness of the 2PI kernel and thereby justifying the short-distance limit in the manner of Appelquist and Poggio, one could also proceed to examine directly the 2PI graphs other than the one-particle exchange and show that they are suppressed relative to the leading-logarithm behavior obtained from one-particle exchange. This will be our approach in the QCD case. This procedure for $(\phi^3)_6$ theory is illustrated in Appendix A.

In the limit (2.1) the Bethe-Salpeter equation for $M(p,q)$, shown graphically in Fig. 1, becomes

$$M(p,q) = \frac{(\ln q^2)^{-1-2\gamma}}{b(q-p)^2} + \frac{1}{b}(\ln q^2)^{-1-2\gamma}\int^{q}\frac{d^6k}{(2\pi)^6 k^4}\frac{M(p,k)(\ln k^2)^{2\gamma}}{(q-k)^2}, \tag{2.5}$$

where the upper limit $k<q$ indicates the fact that the leading behavior in $\ln q$ comes from the region $k \lesssim q$, as one can easily verify by analyzing the first iteration of Eq. (2.5), the box diagram (see Appendix A). The factor $(\ln k^2)^{2\gamma}$ comes from the propagators joining K and M in Fig. 1. We shall consistently analyze the Bethe-Salpeter equation only in this leading-log approximation, which is equivalent to the usual analysis of asymptotic freedom via the renormalization group.[4]

The next step in obtaining the asymptotic solution of Eq. (2.5) is to reduce it to an integral equation in one variable by a partial-wave analysis. The most elegant way to perform the analysis is to exploit the O(6) symmetry of the equation [O(4) in the QCD case] by expanding in O(6) spherical harmonics.[5] We shall instead present the simpler analysis which results when terms of order p^2/q^2 are neglected. Then in the leading-log approximation Eq. (2.5) is diagonalized by the power-series expansion

$$M(p,q) = \frac{1}{bq^2}(\ln q^2)^{-1-2\gamma}\sum_{n=0}^{\infty} M_n(p^2,q^2)\omega^n. \tag{2.6}$$

That this expansion diagonalizes Eq. (2.5) in leading-log approximation follows from the integral

$$\int\frac{d\Omega}{(2\pi)^6}\left(\frac{2p\circ k}{k^2}\right)^m\left(\frac{2q\circ k}{q^2}\right)^n \sim \delta_{mn}\gamma_n\omega^n, \tag{2.7}$$

where γ_n is a positive number depending only on n. The integral vanishes for $n\neq m$ in the following sense: If $m>n$ the result is proportional to p^2, and gives rise to terms of order p^2/q^2, which we neglect; if $n>m$ the result is proportional to k^2/q^2, which does not contribute to the leading $\ln q^2$ order. That is,

$$\int^{q^2}\frac{dk^2}{k^2\ln k^2} \sim \ln\ln q^2,$$

whereas

$$\int^{q^2}\frac{dk^2}{q^2\ln k^2} \sim \frac{1}{\ln q^2}.$$

Performing the angular integrations one then finds that Eq. (2.5) reduces to

$$M_n(p^2,q^2) = 1 + \frac{\gamma_n}{b}\int^{q^2}\frac{dk^2}{k^2}(\ln k^2)^{-1}M_n(p^2,k^2). \tag{2.8}$$

Differentiating with respect to q^2 enables one to solve for the large-q^2 behavior,

$$M_n(p^2,q^2) = F_n(p^2)(\ln q^2)^{\gamma_n/b}, \tag{2.9}$$

where the arbitrary function $F_n(p^2)$ reflects ignorance about the low-k^2 portion of the range of integration. Equation (2.9) shows the emergence of the anomalous dimension in deep-inelastic scattering.

One can in fact determine the behavior of $F_n(p^2)$ for large p^2 by imposing the boundary condition that in the short-distance limit $M(p,q) \sim K(p,q)$, or, using Eq. (2.6),

$$M_n(p^2,q^2) \sim 1 \tag{2.10a}$$

as

$$p=\lambda\hat{p}, \quad q=\lambda\hat{q}, \quad \lambda\to\infty \tag{2.10b}$$

which implies that for large p^2,

$$F_n(p^2) \sim (\ln p^2)^{-\gamma_n/b}. \tag{2.11}$$

Finally, the solution can be written

$$M_n(p^2,q^2) = f_n(p^2)\left(\frac{\ln q^2}{\ln p^2}\right)^{\gamma_n/b}, \tag{2.12a}$$

where the function $f_n(p^2)$ is arbitrary except for the condition

$$f_n(p^2) \sim 1. \tag{2.12b}$$

The large-p^2 behavior can also be imposed as a boundary condition on Eq. (2.8), where it determines the lower limit of integration when p^2 is large,

$$M_n(p^2,q^2) = 1 + \frac{\gamma_n}{b}\int_{p^2}^{q^2}\frac{dk^2}{k^2}(\ln k^2)^{-1}M_n(p^2,k^2). \tag{2.13}$$

One finds that Eq. (2.12) is indeed a solution of Eq. (2.13).

In some applications it will prove to be more convenient to use the Bethe-Salpeter equation iterated in the opposite order (see Fig. 3) which has the asymptotic form in the limit (2.1)

$$M(p,q) = \frac{(\ln q^2)^{-1-2\gamma}}{b(q-p)^2} + \frac{1}{b}\int^{q}\frac{d^6k}{(2\pi)^6 k^6}(\ln k^2)^{-1}M(k,q). \tag{2.14}$$

We shall usually employ this form, which is more closely analogous to the operator-product formalism.

Note that the kernel and intermediate propa-

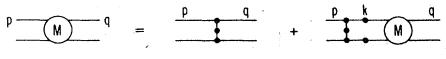

FIG. 3. The "reverse" Bethe-Salpeter equation.

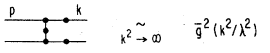

FIG. 4. The asymptotic behavior of the kernel entering the "reverse" Bethe-Salpeter equation of Fig. 3. Note that all propagators and 1PI vertices are evaluated, asymptotically, at k^2.

gators (Fig. 4) entering this "reverse" equation are all evaluated effectively at k^2, and that the correct number of 1PI vertices and propagator renormalizations are present so that

$$K(p,k)D^2(k^2) \sim \frac{1}{k^4}\bar{g}^2(k^2/\lambda^2) \sim \frac{1}{b\,k^4 \ln(k^2/\lambda^2)}. \qquad (2.15)$$

Using the expansion (2.6) one finds the partial-wave equation for large p^2

$$M_n(p^2,q^2) = 1 + \frac{\gamma_n}{b}\int_{p^2}^{q^2}\frac{dk^2}{k^2}(\ln k^2)^{-1}M_n(k^2,q^2). \qquad (2.16)$$

It is easy to verify that (2.12) is indeed the solution of this equation. The fact that the two equations (2.13) and (2.16) are completely equivalent can be seen by recognizing that they both imply that $M_n(p^2,q^2)$ is a function only of the ratio $\xi = \ln q^2/\ln p^2$. A little algebra then allows one to cast either equation in the form

$$M_n(\xi) = 1 + \frac{\gamma_n}{b}\int_1^{\xi}\frac{d\zeta}{\zeta}M_n(\zeta).$$

In order to calculate a reaction such as deep-inelastic scattering one must connect the amplitude M to the full 2PI "current" attachment graph C, [see Fig. 5(a)]. Using either of the approaches discussed above for the 2PI kernel one may establish for C that only the one-particle exchange graph, Fig. 5(b), survives in the leading-log approximation. This yields an equation for the current scattering amplitude A of the form

$$A(p,q) = \frac{(\ln q^2)^{-\gamma}}{(p-q)^2} + (\ln q^2)^{-\gamma}\int^{q}\frac{d^6k}{(2\pi)^6 k^4}\frac{(\ln k^2)^{2\gamma}}{(k-q)^2}M(p,k), \qquad (2.17)$$

which for partial waves becomes to leading log

$$A_n(p^2,q^2) = 1 + \frac{\gamma_n}{b}\int_{p^2}^{q^2}\frac{dk^2}{k^2\ln k^2}\left(\frac{\ln k^2}{\ln p^2}\right)^{\gamma_n/b} = \left(\frac{\ln q^2}{\ln p^2}\right)^{\gamma_n/b}, \qquad (2.18)$$

where we have defined

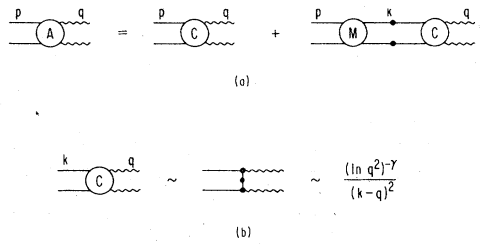

FIG. 5. Connecting the amplitude M to the currents. C is two-particle irreducible and thus has the asymptotic behavior of the one-particle exchange graph, as shown in (b).

$$A(p,q) = \sum_n A_n(p^2,q^2)\frac{(\ln q^2)^{-\gamma}}{q^2}\left(\frac{2p\cdot q}{q^2}\right)^n. \qquad (2.19)$$

Note that in renormalizing the current attachment vertices in such a manner as to define the renormalized charge squared e_R^2, we have to supply a propagator renormalization; thus the one-particle exchange current attachment kernel C has the asymptotic form

$$C(k,q) \sim e_R^2\frac{[\ln(q^2/\lambda^2)]^{-\gamma}}{(k-q)^2}. \qquad (2.20)$$

From Eqs. (2.18) and (2.19) we see that the nth moment F_n of the deep-inelastic structure function $[\mathrm{Im}(q^2A(p,q))/\pi]$, which is the coefficient of ω^n in the expansion of q^2A, behaves as

$$F_n \sim f_n(p^2)(\ln q^2)^{\gamma_n/b-\gamma}. \qquad (2.21)$$

The quantity $\gamma_n/b - \gamma$ is thus the anomalous dimension usually found by using the renormalization group. The p^2 behavior is similarly controlled by the anomalous-dimension combination, $\gamma_n/b - \gamma$, once wave-function renormalization of the initial quark line (with momentum p) is incorporated.

One particularly important point is now apparent. The $(\ln q^2)^{\gamma_n/b}$ powers arising from divergent loop integrations have been separated from the short

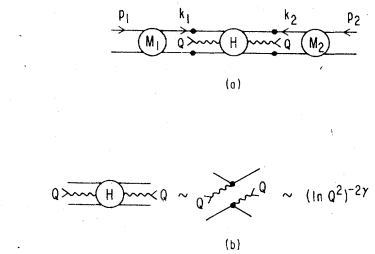

FIG. 6. (a) Massive μ-pair production showing the separation of the kernel H which is 2PI in both of the colliding quark channels. (b) H is infrared finite as k_1^2 and $k_2^2 \to 0$ so that its short-distance limit dominates as $Q^2 \to \infty$.

distance one-particle-exchange limit of the "Born" current attachment graph of Fig. 5(b). This same procedure applies to other parton-model processes. As a second example consider $\mu^+\mu^-$ pair production, Fig. 6(a). The amplitude H describing the attachment of the colliding quarks 1 and 2 to the massive μ pair is defined to be 2PI in the channels of each of the two quarks. It is infrared finite, and thus its leading behavior comes from the short-distance limit of the simplest graph, shown in Fig. 6(b). The full $\mu^+\mu^-$ production amplitude is thus

$$\int \frac{d^6k_1}{(2\pi)^6} \frac{M_1(p_1,k_1)}{k_1^4} (\ln k_1^2)^{2\gamma} \int \frac{d^6k_2}{(2\pi)^6} \frac{M_2(p_2,k_2)}{k_2^4} (\ln k_2^2)^{2\gamma} H(k_1,k_2,Q), \tag{2.22}$$

with

$$H(k_1,k_2,Q) \sim (\text{standard bare diagram with renormalized charges}) (\ln Q^2)^{-(\gamma_1+\gamma_2=2\gamma)}. \tag{2.23}$$

Note that we have again isolated the scale violations resulting from the accumulating logarithmic divergences in the amplitudes M_1 and M_2, which are measured in deep-inelastic current experiments. Equations (2.22) and (2.23) thus imply that the standard Drell-Yan[6] formula is applicable for the leading-log behavior of $\mu^+\mu^-$ pair production provided that quark distributions incorporating the leading-log scale violations are used. The fact that the amplitude which is two-particle irreducible in both of the quark channels may be asymptotically approximated by its simplest "Born" contribution with properly renormalized vertices and propagators is crucial.

Note how two factors of $(\ln Q^2)^\gamma$, one for each quark participating in the "Born" process, must be supplied in order to correctly define the renormalized couplings inside the "Born" amplitude [Eq. (2.23)]. Thus *two* factors of $(\ln Q^2)^{-\gamma}$ appear in Eq. (2.23) and are absorbed into the behavior of the *two* colliding quark distributions, just as occurred in the deep-inelastic current case. We again obtain quark distributions characterized by anomalous dimensions $\gamma_n/b - \gamma$, where γ_n/b comes from M and γ comes from renormalization of the "Born" quark amplitude.

This procedure generalizes to high p_T and other short-distance processes. A factor $(\ln "Q^{2"})^\gamma$ for each participating initial or final quark must be absorbed into the 2PI Born graph in order that all couplings in that graph are correctly renormalized at the moving point "Q^2" associated with the kernel (of course for a high-p_T subprocess "Q^2" is of order $4p_T^2$). The leftover $(\ln "Q^{2"})^{-\gamma}$ factor is combined with the leading-logarithmic behavior obtained from the amplitude M, describing the connection of a given initial- or final-state quark to its associated initial- or final-state hadron, to yield the standard scale-broken quark emission or decay probabilities.

III. DIAGRAMMATIC METHOD FOR DEEP-INELASTIC SCATTERING IN QCD

A. Lipatov Gauge

Extension to QCD of the diagrammatic method of analyzing deep-inelastic scattering in leading-log approximation is straightforward, provided that a certain gauge is chosen. Unless a special gauge choice is made, one finds that ladder diagrams are not the only contributors to leading-log approximation.

To be specific, let us consider the problem of deep-inelastic scattering off spin-averaged quarks. That is, we wish to evaluate the amplitude corresponding to the diagram in Fig. 7(a). As before, we first perform the evaluation in the limit $q^2 \to \infty$ with $2p\cdot q/q^2 \equiv \omega \to 0$, and with $p^2 = 0$. The straightforward extension of the Bethe-Salpeter equation of Fig. 4 would be given by the ladder diagrams of Fig. 8. In QCD, however, diagrams such as that shown in Fig. 9, in which a gluon emanates from the interior of a vertex, can contribute to the leading-log behavior.

To analyze such contributions in detail, let us consider the subdiagram shown in Fig. 10. If one is given the amplitude for $q\bar{q} \to \gamma^*\gamma^*$ [Fig. 7(a)] in the form of a power series in ω,

$$F(p,q) = \frac{\not{q}}{q^2} \sum_{n=0}^{\infty} f_n(p^2,q^2) \left(\frac{2p\cdot q}{q^2}\right)^n, \tag{3.1}$$

then one can generate the amplitude for $q + \bar{q} +$ gluon $\to \gamma^* + \gamma^*$ (Fig. 10), by the minimal-coupling prescription (letting $p \to p + k$, extracting coefficient of k_μ). One obtains

FIG. 7. Fermion and gluon amplitudes.

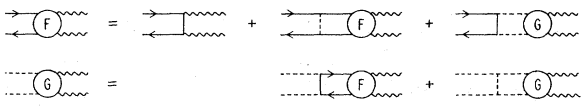

FIG. 8. (a) Bethe-Salpeter equation for F. (b) Bethe-Salpeter equation for G. Full vertex and propagator renormalization blobs are understood to be present on all internal lines.

$$-\frac{2q_\mu \not{q}}{q^4}\sum_{n=1}^{\infty} f_n(p^2,q^2)\sum_{k=1}^{n}\left(\frac{2q\cdot p}{q^2}\right)^{n-k}\left(\frac{2q\cdot k}{q^2}\right)^{k-1}\binom{n}{k}. \tag{3.2}$$

Additional terms which arise in both Eq. (3.1) and Eq. (3.2) do not contribute to the leading-log order; for example, terms proportional to $\not{p}$ rather than $\not{q}$ in Eq. (3.1) can easily be found to be negligible in leading-log approximation when substituted into the Bether-Salpeter equation of Fig. 8.

Now the crucial observation is that these internal gluon-emission amplitudes, such as Eq. (3.2), are proportional in leading-log approximation to q_μ. If, therefore, the gauge is chosen in which the gluon polarization vector ϵ is orthogonal to q,

$$\epsilon\cdot q = 0, \tag{3.3}$$

then the internal gluon-emission diagrams such as Fig. 9 will vanish to this order. Since a similar axial gauge was used by Lipatov in order to eliminate nonplanar diagrams, we shall refer to this as Lipatov gauge.[7] In such a gauge the naive ladder-type Bethe-Salpeter graphs of Fig. 8 give the correct leading-log result. Although we shall use Lipatov gauge hereafter, we remark that it is not impossible to work in other gauges. In that case, one can add the nonvanishing diagrams of Fig. 9 to those in Fig. 8, and determine the internal gluon emission amplitudes by the minimal-coupling prescription, as in Eq. (3.3). Diagrams in which more than one internal gluon is emitted are higher order in α_s and do not contribute to the leading-log behavior.

Similar procedures applied to the (singlet) gluon channels prove that only the $gg\to\gamma^*\gamma^*$ amplitude contributes in leading log. The ability

FIG. 9. A possibly important diagram in QCD. Internal gluon emission amplitudes such as this survive in the leading logarithmic behavior if the Feynman gauge is employed, but are nonleading in axial gauges.

FIG. 10. The amplitude for 1-gluon emission from a $q\bar{q}\to\gamma^*\gamma^*$ amplitude.

to use gauge invariance to generate the gluon coupling amplitude in fact simplifies the leading-log "ladderization" proof relative to the ϕ^3 case.

In Lipatov gauge the propagator of a gluon of momentum k is given by

$$D_{\mu\nu}(k) = \frac{1}{k^2}\left[-g_{\mu\nu}+\frac{q_\mu k_\nu + k_\mu q_\nu}{q\cdot k}-\frac{q^2 k_\mu k_\nu}{(q\cdot k)^2}\right] \equiv \frac{P_{\mu\nu}(k)}{k^2}. \tag{3.4}$$

The singularities at $q\cdot k=0$ can be handled by the principal-value prescription of Kaintz, Kummer, and Schweda (KKS).[8]

B. Calculation of W_1

Making the usual decomposition ($\nu = p\cdot q$)

$$W_{\mu\nu}(p,q) = -W_1(\nu,q^2)\left(g_{\mu\nu}-\frac{q_\mu q_\nu}{q^2}\right) + W_2(\nu,q^2)\left(p_\mu-\frac{\nu q_\mu}{q^2}\right)\left(p_\nu-\frac{\nu q_\nu}{q^2}\right). \tag{3.5}$$

We consider in this section the calculation of the transverse structure function W_1, and defer to the next section the calculation of the longitudinal structure function

$$W_L \sim \tfrac{1}{2}\nu\omega W_2 - W_1, \tag{3.6}$$

which vanishes in leading-log approximation.

The Bethe-Salpeter equations for W_1, shown diagrammatically in Fig. 8, are diagonalized in leading-log approximation by expansions, which generalize Eq. (2.6),

$$F_1(p,q) = \delta_{ab}\delta_{ij}\not{q}\sum_{n=2}^{\infty} f_{1,n}^{i}(p^2,q^2)\omega^{n-1}/q^2, \tag{3.7a}$$

$$G_1(p,q) = \delta_{ab}g_{\delta\tau}\nu\sum_{n=2}^{\infty} g_{1,n}(p^2,q^2)\omega^{n-1}/q^2. \tag{3.7b}$$

where i,j are flavor, a,b are color, and δ,τ are Lorentz indices. As remarked above, terms proportional to $\not{p}$ in F do not contribute to leading log. The relatively simple form of G given above comes about as follows: Gauge invariance requires that the on-shell limit of $G_1(k,q)$ be proportional to

$$g_{\delta\tau}-\frac{k_\delta q_\tau + k_\tau q_\delta}{q\cdot k}+O(k^2,k_\delta k_\tau). \tag{3.8}$$

The terms of order k^2 or $k_\delta k_\tau$ do not contribute to leading log. Moreover, the second term above does not contribute since we employ the Lipatov gauge for intermediate gluon propagators in the ladder. The amplitude G is, therefore, effectively proportional to $g_{\delta\tau}$, as stated in Eq. (3.7b).

Using the expansions given in Eq. (3.7) to simplify the Bethe-Salpeter equations of Fig. 8 results, as before, in equations diagonal in the index n, in leading-log approximation. The performance of the loop integrals is identical to the calculation of critical exponents. See especially Gross and Wilczek, Appendix B.[4] Note also the analogy between the diagrams of Fig. 2 of that reference and our Fig. 8. The only difference is that working in Lipatov gauge eliminates three of the seven diagrams, but of course the more complicated propagator (3.4) reintroduces a comparable level of complexity. Sample calculations are given in Appendix B. The result is the coupled equations

$$f^i_{\alpha,n}(p^2,q^2)=F^i_{\alpha,n}(\ln q^2)^{-\bar\gamma_F}+\frac{b^n_{FF}}{b}\int_{p^2}^{q^2}\frac{dk^2}{k^2}(\ln k^2)^{-1}f^i_{\alpha,n}(k^2,q^2)+\frac{b^n_{FG}}{b}\int_{p^2}^{q^2}\frac{dk^2}{k^2}(\ln k^2)^{-1+\bar\gamma_G-\bar\gamma_F}g_{\alpha,n}(k^2,q^2)\,, \tag{3.9a}$$

$$g_{\alpha,n}(p^2,q^2)=G_{\alpha,n}(\ln q^2)^{-\bar\gamma_G}+\frac{b^n_{GF}}{b}\int_{p^2}^{q^2}\frac{dk^2}{k^2}(\ln k^2)^{-1+\bar\gamma_F-\bar\gamma_G}\sum_i f^i_{\alpha,n}(k^2,q^2)$$

$$+\frac{b^n_{GG}}{b}\int_{p^2}^{q^2}\frac{dk^2}{k^2}(\ln k^2)^{-1}g_{\alpha,n}(k^2,q^2)\,. \tag{3.9b}$$

We follow the notation of Politzer[9]; the b^n_{IJ} differ from the usual anomalous dimensions γ^n_{IJ} in that the latter include contributions of self-energy diagrams whereas the former do not; the quantities $\bar\gamma_I$ are defined as $\bar\gamma_I=\gamma_I/b$, where γ_I is the self-energy piece in Politzer's notation. The subscript $\alpha=1,L$ designates transverse or longitudinal structure function. For the transverse case we are considering at present, the inhomogeneous terms given by the tree graph in Fig. 6 are simply[10]

$$F^i_{1,n}=2Q_i^2\,,\quad G_{1,n}=0\,, \tag{3.9c}$$

where Q_i is the charge (in units of e) on the ith quark. The values of the γ's and b's are listed in Appendix B. The diagonal term b_{FF} and the associated γ_F differ from those obtained, say, in Feynman gauge. However, the combination $b_{FF}-\gamma_F$ associated with the anomalous dimension of the gauge-invariant operator W_1 yields the standard result. The importance of considering such combinations is even more apparent in the Altarelli-Parisi scheme where b^n_{FF} γ_F b^n_{GG} and γ_G are all separately infinite.

As usual, one must treat singlet and nonsinglet amplitudes separately. The singlet case, which is considerably more complicated, is relegated to Appendix C. Defining nonsinglet amplitudes $f^{ij}=f^i-f^j$, $i\neq j$, one sees that (3.9) simplifies to

$$f^{ij}_{\alpha,n}(p^2,q^2)=F^{ij}_\alpha(\ln q^2)^{-\bar\gamma_F}+\frac{b^n_{FF}}{b}\int_{p^2}^{q^2}\frac{dk^2}{k^2}(\ln k^2)^{-1}f^{ij}_{\alpha,n}(k^2,q^2)\,. \tag{3.10}$$

This equation, which is essentially identical to Eq. (2.13) encountered in the $(\phi^3)_6$ model, has the solution

$$f^{ij}_{\alpha,n}(p^2,q^2)=F^{ij}_\alpha A_n(p^2)(\ln q^2)^{-\gamma^n_{FF}/2b}(\ln p^2)^{-b^n_{FF}/b}\,, \tag{3.11}$$

where

$$\gamma^n_{IJ}=-2b^n_{IJ}+2\gamma_I\delta_{IJ}\,, \tag{3.12}$$

and where, as in Eq. (2.12), the function $A_n(p^2)$ is unknown except for the restriction

$$A_n(p^2)\sim 1\,. \tag{3.13}$$

One finds T_α, the forward spin-averaged amplitude for Compton scattering off quarks, from F_α by taking the spin average, $T_\alpha=\frac{1}{2}\mathrm{Tr}(\not{p}F_\alpha)$ to obtain

$$T_\alpha(\nu,q^2)=\sum_{n=0}^{\infty}f_{\alpha,n}(p^2,q^2)\omega^n\,. \tag{3.14}$$

We now employ the standard theorem which states that the expansion coefficients of the amplitude T_α in powers of ω are related to the moments of

the structure function $W_\alpha \equiv \mathrm{Im}\, T_\alpha/2\pi$; i.e. $(x = 1/\omega)$

$$\int_0^1 W_\alpha(x, q^2) x^{n-1} dx = \tfrac{1}{4} f_{\alpha,n}(p^2, q^2). \tag{3.15}$$

Thus Eq. (3.11) reproduces the well-known result of logarithmic scaling violation in QCD.[4] The asymptotic p^2 dependence is written out in more detail than usual, because it will be convenient to integrate over p^2 in subsequent applications.

C. Calculation of W_L

The calculation of W_L introduces some interesting new features, in that this amplitude vanishes in the leading-log approximation we have been considering. The inhomogeneous term in Fig. 8 coming from the tree graph gives zero (i.e., order $1/q^2$) contribution to W_L, and therefore, the leading-log ladder graphs we have been summing give zero contribution.

The longitudinal structure function W_L can be projected by the operation

$$p_\mu p_\nu W_{\mu\nu} = \tfrac{1}{2} \nu\omega W_L(p, q). \tag{3.16}$$

In solving the Bethe-Salpeter equation, we shall need to consider amplitudes $F_L(k, q)$ for quarks with intermediate momenta k, whereas the projection of W_L in (3.16) involves the final momentum p. To avoid confusion, let us consider the quantity

$$W_L(\Delta; p, q) = \Delta_\mu \Delta_\nu W_{\mu\nu}(p, q), \tag{3.17}$$

which will yield $W_L(p, q) = W_L(p; p, q)$ at the end of the calculation when Δ_μ is set equal to p_μ. Since there is now a third four-vector Δ on which $W_L(\Delta; p, q)$ depends bilinearly, there are eight possible structures for this amplitude:

$$\begin{aligned} &\not{\Delta} p\cdot\Delta, \quad \not{p} p\cdot\Delta\, q\cdot\Delta, \quad \not{p}(p\cdot\Delta)^2, \\ &\not{q} q\cdot\Delta\, p\cdot\Delta, \quad \not{q}(p\cdot\Delta)^2, \\ &\not{\Delta} q\cdot\Delta, \quad \not{p}(q\cdot\Delta)^2, \\ &\not{q}(q\cdot\Delta)^2. \end{aligned} \tag{3.18}$$

The first five of these vanish when $\Delta \to p$, since we are taking $p^2 = 0$ (that is, neglecting mass corrections such as p^2/q^2). The next two vanish for spin-averaged quarks, and we conclude that only the last structure, $\not{q}(q\cdot\Delta)^2$, gives a nonvanishing contribution to W_L off spin-averaged quarks. The tree graphs in Fig. 8 give, however, no contribution to this structure. Moreover, it is not difficult to show that *none* of the first seven structures in (3.18) when iterated in the Bethe-Salpeter equation yields any contribution to this structure. Thus W_L vanishes in the leading-log ladder-graph approximation, as stated.

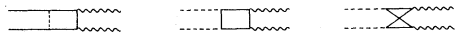

FIG. 11. The inhomogeneous terms contributing to the $\not{q}(q\cdot\Delta)^2$ structure necessary for W_L.

Nonvanishing contributions to W_L must involve loss of the leading logarithm in at least one loop integral. The leading contribution to W_L will involve such loss in only one loop integral. Moreover, we show in Appendix D that this must occur in the *first* loop, the one nearest the hard photons. The diagrams which contribute are shown in Fig. 11. What happens, then, is that these diagrams give a nonvanishing contribution proportional to $\not{q}(q\cdot\Delta)^2$. It is easy to verify that this form, once generated, propagates unchanged through successive iterations of the Bethe-Salpeter equation (in leading-log approximation, which we reinstate after obtaining the nonleading contribution of the first loop only). Thus we need consider amplitudes of only this form, and can ignore the first seven structures in (3.18). For the longitudinal amplitude we thus write, instead of Eq. (3.7),

$$F_L = \delta_{ab}\delta_{ij}\not{q}\,\frac{(q\cdot\Delta)^2}{q^4}\sum_n f^i_{L,n}(p^2, q^2)\omega^{n-1}, \tag{3.19a}$$

$$G_L = \delta_{ab} g_{\delta\tau\nu}\,\frac{(q\cdot\Delta)^2}{q^4}\sum_n g_{L,n}(p^2, q^2)\omega^{n-1}. \tag{3.19b}$$

Substituting these expansions in the Bethe-Salpeter equation, given by Fig. 6, one again finds Eq. (3.9) but with the inhomogeneous terms calculated from the diagrams of Fig. 11 (see Ref. 10)

$$F^i_{L,n} = \frac{Q_i^2 C_2(R)}{2\pi^2 b \ln q^2}\,\frac{1}{n+1}, \tag{3.20a}$$

$$G_{L,n} = \frac{2\sum_{i=1}^{n_f} Q_i^2 T(R)}{\pi^2 b \ln q^2}\,\frac{1}{(n+1)(n+2)}. \tag{3.20b}$$

The solution of these integral equations is exactly as for W_1, with the only difference being in the inhomogeneous terms. The singlet case is discussed in Appendix C, the nonsinglet solution is given in Eq. (3.11). From Eqs. (3.11), (3.9c), and (3.20) we recover the usual result[11]

$$\frac{\int_0^1 W_L^{\mathrm{ns}}(x, q^2) x^{n-1} dx}{\int_0^1 W_1^{\mathrm{ns}}(x, q^2) x^{n-1} dx} = \frac{F^{\mathrm{ns}}_{L,n}}{F^{\mathrm{ns}}_{1,n}} = \frac{C_2(R)}{4\pi^2 b \ln q^2 (n+1)}. \tag{3.21}$$

Our analysis of deep-inelastic scattering off quarks, having yielded all the usual results as a test of our diagrammatic method, is now complete.

IV. DERIVATION OF THE ALTARELLI-PARISI SCHEME

We will now employ the Lipatov gauge (or, more generally, any axial gauge with the trace of the gluon propagator being -2 in a leading-log sense) and our Bethe-Salpeter techniques to derive and justify the scheme proposed by Altarelli and Parisi[2] (AP) for understanding asymptotic freedom. Several ingredients in their paper are *ad hoc*; these include: (a) the calculation only of bremsstrahlung (in our language, "ladder") contributions; and (b) the regularization of the divergent moments of the bremsstrahlung calculations in the prescribed fashion. Moreover, the "master equation," on which their method is based, they obtain from the standard operator-product, renormalization-group result. We shall see that all these ingredients emerge naturally in our approach.

We have already proven that the ladder approximation gives the leading logarithmic result when axial gauge is employed. Also the moving coupling constant is incorporated into the kernels and Born terms of our Bethe-Salpeter equation. In fact, we need only show that there is a particular method for computing the anomalous dimensions arising from the ladder Bethe-Salpeter equation which looks like that used by AP; their method differs in the choice of a regularization scheme other than that of KKS used in Secs. II and III, and in delaying diagonalization of the Bethe-Salpeter equation to a later stage of the calculation.

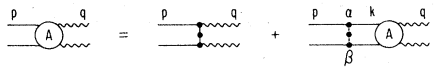

FIG. 12. The nonsinglet reverse Bethe-Salpeter equation.

We shall concentrate on the nonsinglet case. The reverse Bethe-Salpeter equation for $q\bar{q} \to \gamma^*\gamma^*$ in the fermion nonsinglet channel is, dropping the trivial charge factors for simplicity, (see Fig. 12)

$$A(p,q) = \frac{(\ln q^2)^{-\bar{\gamma}_F}}{(p-q)^2}(\not{p}-\not{q}) + \left(\frac{4}{3}\right)\int \frac{d^4k}{(2\pi)^4(p-k)^2}\frac{P_{\alpha\beta}(p-k)\gamma_\alpha \not{k} A(k,q)\not{k}\gamma_\beta}{k^4 b \ln k^2}, \tag{4.1}$$

where $P_{\alpha\beta}$ is defined in Eq. (3.4) and where we have taken the $W_1(\equiv -\frac{1}{2}g_{\mu\nu}W\mu\nu)$ projection. The $(\frac{4}{3})$ is the color group factor $C_2(R)$. We write $A(p,q)$ as

$$A(p,q) = a(p^2,q^2,2p\circ q)\not{p} + b(p^2,q^2,2p\cdot q)\not{q}. \tag{4.2}$$

For convenience we spin average; only the $\not{q}$ parts will survive, as usual. Thus

$$\tfrac{1}{2}\mathrm{Tr}[A\not{p}] \sim 2p\cdot q b, \quad \tfrac{1}{2}\mathrm{Tr}[\not{p}(\not{p}-\not{q})] \sim -2p\cdot q\,. \tag{4.3}$$

For the internal part of the Bethe-Salpeter equation it is pedagogically useful to separate the

$$-g_{\alpha\beta}\ \text{(a)}, \quad \frac{(p-k)_\alpha q_\beta + (p-k)_\beta q_\alpha}{(p-k)\cdot q}\ \text{(b)}, \quad \text{and} \quad -\frac{(p-k)_\alpha (p-k)_\beta q^2}{[(p-k)\cdot q]^2}\ \text{(c)}$$

parts of $P_{\alpha\beta}(p-k)$. We then obtain

$$\begin{aligned}
&\tfrac{1}{2}\mathrm{Tr}[\not{p}\gamma_\alpha \not{k} A(k,q)\not{k}\gamma_\beta]P_{\alpha\beta}(p-k) \\
&\quad = k^2\Bigg\{\left(a + b\frac{2q\cdot k}{k^2}\right)4p\cdot k - 4q\cdot p b && \text{(a)} \\
&\qquad + \frac{1}{(p-k)\cdot q}\left[\left(a+b\frac{2q\cdot k}{k^2}\right)[(2p\cdot k - 2k^2)2p\circ q - 2q\cdot k 2k\cdot p - 2(p-k)\circ q 2p\cdot k] - 2bq^2(-2p\circ k)\right] && \text{(b)} \\
&\qquad + \frac{q^2(-2p\cdot k)}{[(p-k)\cdot q]^2}\left[\left(a+b\frac{2q\cdot k}{k^2}\right)2(p-k)\circ k - 2b(p-k)\circ q\right]\Bigg\}. && \text{(c)}
\end{aligned} \tag{4.4}$$

This structure simplifies greatly if "light-cone" techniques are used to evaluate the d^4k integral of Eq. (4.1). We use the light-cone frame[12]

$$p = \left(P + \frac{M^2}{4P}, 0, P - \frac{M^2}{4P}\right), \quad q = \left(\frac{\nu}{2P}, \vec{q}_\perp, -\frac{\nu}{2P}\right), \quad k = \left(zP + \frac{k^2+k_\perp^2}{4zP}, \vec{k}_\perp, zP - \frac{k^2+k_\perp^2}{4zP}\right), \tag{4.5}$$

and the method of performing the dk^2 integration by picking up the pole in k^2 in the $(p-k)^{-2}$ propagator, i.e.,

$$\int \frac{d^4k f(k^2, k\cdot q)}{(p-k)^2} = \int \frac{dk^2}{2z} dz\, d^2k_\perp \frac{f(k^2, k\cdot q)}{(p-k)^2}$$
$$= \pi \int_0^1 \frac{dz}{1-z} d^2k_\perp f\left(k^2 = zM^2 - \frac{k_\perp^2}{1-z},\ k\cdot q = zp\cdot q\right), \tag{4.6}$$

where we define for future use

$$x = \frac{q_\perp^2}{2p\cdot q}.$$

Note that $2p\cdot k \sim k^2 \sim -k_\perp^2/(1-z)$ for $p^2 = M^2 \to 0$. The limits on the z integral come from requiring that the singularity structures of $f(k^2, k\cdot q)$ lie on the opposite side of the k^2 axis from that of $1/(p-k)^2$. Following the line of argument presented in Secs. II and III we find that the important range of integration is

$$k_\perp^2 < q_\perp^2 = -q^2. \tag{4.7}$$

The leading-log contribution we seek will have the final structure

$$\int^{q_\perp^2} \frac{dk_\perp^2}{k_\perp^2} \frac{1}{b \ln k_\perp^2}. \tag{4.8}$$

Corrections to the integrand of order $k_\perp^2/q_\perp^2$ do not contribute to the leading log;

$$\int^{q_\perp^2} \frac{dk_\perp^2}{k_\perp^2} \frac{k_\perp^2}{q_\perp^2} \frac{1}{b \ln k_\perp^2} \sim \frac{1}{b \ln q_\perp^2}. \tag{4.9}$$

With this in mind one can greatly simplify the trace structure (4.4). We obtain in the leading-logarithmic approximation

$$\tfrac{1}{2}\mathrm{Tr}[\not{p}\gamma_\alpha \not{k} A(k,q) \not{k}\gamma_\beta] P_{\alpha\beta}(p-k) \sim k^2 \times \begin{cases} 4bp\cdot q(z-1) & \text{(a)} \\ -8\dfrac{bp\cdot qz}{1-z} & \text{(b)} \\ O(1), \text{ not } O(p\cdot q). & \text{(c)} \end{cases} \tag{4.10}$$

The above forms obtain under the leading-log approximations

$$2k\cdot q \sim 2zp\cdot q, \quad (p-k)\cdot q \sim (1-z)p\cdot q,$$

the latter being the source of the $(1-z)^{-1}$ behavior in (4.10). The singular behavior is only apparent but will require temporary regularization as we discuss shortly.

Inserting (4.10) into our integral equation (4.1), using (4.6), and defining $b' = 2p\cdot q b$, we have

$$b'(p,q) = -\frac{2p\cdot q}{(p-q)^2} (\ln q^2)^{-\bar{\gamma}_F} + \left(\frac{4}{3}\right) \int \frac{dz}{8\pi^2} \frac{1+z^2}{1-z} \frac{1}{z} \int^{q_\perp^2} \frac{dk_\perp^2}{b \ln k_\perp^2} \frac{b'(k,q)}{k_\perp^2}. \tag{4.11}$$

We obtain $W_1(q^2, p^2, x)$ by taking $\mathrm{Im} b'(p,q)/2\pi$ to yield [recall $k^2 = -k_\perp^2/(1-z) + zp^2$ and $q^2 = -q_\perp^2$]

$$W_1(q^2, p^2, x) = -\tfrac{1}{2}\delta(x-1)(\ln q_\perp^2)^{-\bar{\gamma}_F} + \left(\frac{4}{3}\right) \int_x^1 \frac{dz}{8\pi^2 z} \frac{1+z^2}{1-z} \int^{q_\perp^2} \frac{dk_\perp^2}{k_\perp^2 b \ln k_\perp^2} W_1\left(q^2, k^2, \frac{x}{z}\right). \tag{4.12}$$

This is the key equation. The various pieces of the trace structure (4.10) have combined together to give the bremsstrahlung structure

$$W_1(q^2, p^2, x) = -\tfrac{1}{2}\delta(x-1)(\ln q_\perp^2)^{-\bar{\gamma}_F} + \int^{q_\perp^2} dk_\perp^2 \int_x^1 \frac{dz}{z} G_{q/q}(z, k_\perp^2) W_1\left(q^2, k^2, \frac{x}{z}\right), \tag{4.13}$$

where

$$G_{q/q}(z, k_\perp^2) \sim \frac{4}{3} \frac{\alpha_s(k_\perp^2)}{2\pi} \frac{1+z^2}{1-z} \frac{1}{k_\perp^2} \tag{4.14a}$$

and

$$\alpha_s(k_\perp^2) \equiv \frac{\bar{g}^2(k_\perp^2)}{4\pi} \sim \frac{1}{4\pi b \ln k_\perp^2}. \tag{4.14b}$$

$G_{q/q}(z, k_\perp^2)$ is the probability for emission of a secondary quark q with fractional longitudinal mo-

mentum z and transverse momentum $k_\perp$ from a primary quark. The Bethe-Salpeter equation has instructed us to employ the moving coupling constant $\alpha_s(k_\perp^2)$ in $G_{q/q}$. We may now diagonalize Eq. (4.13) by taking moments

$$\int_0^1 x^{n-1} W_1(q^2,p^2,x)\cdot dx = \tfrac{1}{4} f_{1,n}(q^2,p^2)\,, \tag{4.15}$$

with the result

$$f_{1,n}(q^2,p^2) = 2(\ln q_\perp^2)^{-\bar\gamma_F} + \frac{b^n_{FF}}{b}\int^{\ln q_\perp^2} \frac{d\ln k_\perp^2}{\ln k_\perp^2} f_{1,n}(q^2,k^2)\,, \tag{4.16}$$

where

$$b^n_{FF} = \lim_{\epsilon\to 0}\int_0^{1-\epsilon} dz z^{n-1}\frac{1+z^2}{1-z}\,\frac{1}{8\pi^2}\left(\frac{4}{3}\right). \tag{4.17}$$

In writing (4.16) we have incorporated the trivial sign change of the Born term necessitated by our unconventional choice for the direction of q (see Ref. 10). Note that b^n_{FF} is logarithmically divergent as $z\to 1$, in our leading-log light-cone approximation, and that we must momentarily insert a cutoff to keep $z<1-\epsilon$. This infrared divergence comes from the second term of $P_{\alpha\beta}$ present in an axial gauge. The solution to (4.16) is

$$f_{1,n}(q^2,k^2) \sim 2(\ln q_\perp^2)^{b^n_{FF}/b-\bar\gamma_F}(\ln k_\perp^2)^{-b^n_{FF}/b}. \tag{4.18}$$

Thus the experimentally meaningful quantity is the anomalous dimension of the gauge-invariant operator W_1,

$$\frac{\gamma^n_{FF}}{2b} \equiv -\frac{b^n_{FF}}{b} + \bar\gamma_F \tag{4.19}$$

[see Eq. (3.14)] and not b^n_{FF} itself. In fact a simple calculation in Appendix E using the same integration techniques yields

$$\bar\gamma_F = \frac{1}{8\pi^2 b}\lim_{\epsilon\to 0}\int_0^{1-\epsilon} dz\,\frac{1+z^2}{1-z}\left(\frac{4}{3}\right), \tag{4.20}$$

i.e., an unweighted integral over $G_{q/q}(z)$, so that

$$\frac{\gamma^n_{FF}}{2b} = \left(\frac{4}{3}\right)\frac{(-1)}{8\pi^2 b}\int_0^1 dz(z^{n-1}-1)\frac{1+z^2}{1-z} \tag{4.21a}$$

$$= +\frac{1}{16\pi^2 b}\left(\frac{4}{3}\right)\left(1-\frac{2}{n(n+1)}+4\sum_{j=2}^{n}\frac{1}{j}\right). \tag{4.21b}$$

Note that the $z\to 1$ singularities have canceled between b^n_{FF}/b and $\bar\gamma_F$, allowing us to take $\epsilon\to 0$, and the standard[4] result (4.21b) is obtained after a few simple algebraic maneuvers. Thus we have seen that the AP regularization scheme is actually accomplished by properly including the wave-function renormalization effects. The anomalous dimension $\gamma^n_{FF}/2b$ is independent of regularization scheme and integration techniques, but its two components b^n_{FF}/b and $\bar\gamma_F$ depend strongly on the approach employed. Needless to say b^n_{GG}/b and $\bar\gamma_G$ display similar divergences to those encountered above, but again the combination is finite and yields the usual result. The AP expressions for b^n_{FG} and b^n_{GF} are finite. Sample light-cone technique calculations of b^n_{FG} and b^n_{GF} are given in Appendix E. One quickly discovers that in these cases the contributing trace terms are the same in the light-cone technique as in the earlier technique of Sec. III based on KKS regularization. We summarize the results below:

$$b^n_{FF} = \frac{1}{8\pi^2}\int_0^1 z^{n-1}dz\left(\frac{1+z^2}{1-z}\right)\left(\frac{4}{3}\right),$$

$$\gamma_F = \frac{1}{8\pi^2}\int_0^1 dz\left(\frac{1+z^2}{1-z}\right)\left(\frac{4}{3}\right),$$

$$b^n_{GF} = \frac{-2}{8\pi^2}\int_0^1 dz 2[z^2+(1-z)^2]z^{n-1}\left(\frac{1}{2}\right)$$

$$= \frac{-4}{8\pi^2}\,\frac{n^2+n+2}{n(n+1)(n+2)}\left(\frac{1}{2}\right),$$

$$b^n_{FG} = -\frac{1}{16\pi^2}\int_0^1 dz\left(\frac{1+(1-z)^2}{z}\right)z^{n-1}\left(\frac{4}{3}\right) \tag{4.22}$$

$$= -\frac{1}{16\pi^2}\frac{n^2+n+2}{n(n^2-1)}\,\frac{4}{3}\,,$$

$$b^n_{GG} = \frac{1}{8\pi^2}\int_0^1 dz 2\left(\frac{z}{1-z}+\frac{(1-z)}{z}+z(1-z)\right)z^{n-1}(3),$$

$$\gamma_G = \frac{1}{8\pi^2}\int_0^1 dz 2\left(\frac{z}{1-z}+\frac{1-z}{z}+z(1-z)\right)z(3)$$

$$+\frac{1}{8\pi^2}\int dz[z^2+(1-z)^2]n_f\left(\frac{1}{2}\right),$$

with

$$b^n_{FF}-\gamma_F = -\frac{1}{16\pi^2}\left(1-\frac{2}{n(n+1)}+4\sum_{j=2}^{n}\frac{1}{j}\right)\left(\frac{4}{3}\right),$$

$$b^n_{GG}-\gamma_G \tag{4.23}$$

$$= -\frac{1}{16\pi^2}\left(-\frac{4}{n(n-1)}-\frac{4}{(n+1)(n+2)}\right.$$

$$\left.+4\sum_{j=2}^{n}\frac{1}{j}+\frac{1}{3}\right)(3)-\frac{1}{16\pi^2}\,\frac{4}{3}\,n_f\left(\frac{1}{2}\right).$$

We have inserted the group-theoretical constants $C_2(G)=(3)$, $C_2(R)=(\frac{4}{3})$ and $T(R)=(\frac{1}{2})$ per fermion flavor. Up to this point we have carefully avoided discussing γ_G and b^n_{GG} in detail in either the light-cone or KKS regularization approaches. These calculations are clearly somewhat lengthier than those presented. A brief outline of the interesting details appears in Appendix F. We have written the gluon part of γ_G in such a way as to make the cancellation of its divergences with those of b^n_{GG} apparent. This is discussed further in Appendix F.

V. DISCUSSION

We have developed a method for diagrammatic analysis of deep-inelastic scattering in QCD. In a particular axial gauge, which we call the Lipatov gauge, the leading contributions come from ladder graphs obtained from iteration of the Bethe-Salpeter equation corresponding to Fig. 8. Typical diagrams contributing to leading behavior are ladders such as in Fig. 13(a). The analytic expressions corresponding to these diagrams are obtained by solving the Bethe-Salpeter equation. This equation is reduced to a simple integral equation in one variable by expanding in $O(4)$ partial waves, or, more simply, by a power-series expansion in $\omega=2p\cdot q/q^2$. This expansion corresponds to the operator-product expansion in the usual formalism.[4] The close analogy of the two methods is further shown by the correspondence between the Bethe-Salpeter diagrams in Fig. 8 and the diagrams used in calculating the anomalous dimensions in the renormalization-group approach.

The calculation of a process which vanishes in leading order, such as the longitudinal structure function, differs only in the form of the inhomogeneous term in the Bethe-Salpeter equation. Those shown in Fig. 11 are the contributors to W_L. A typical diagram which results is shown in Fig. 13(b). One finds that the leading contribution comes when only one loop integral loses its leading logarithm; moreover, that loop must be the one nearest the hard photons. Hence those shown in Fig. 11 are the only possibilities. Since the contribution of these loops to W_L is not of leading-log order, use of the Lipatov gauge no longer eliminates nonplanar graphs and the crossed loop can occur at the top of the ladder in Fig. 13.

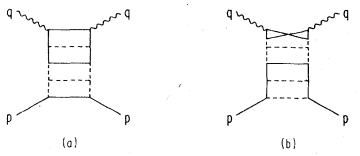

FIG. 13. Typical graphs contributing (a) to W_1, (b) to W_L.

Although it is gratifying that our method reproduces the usual results, it is appropriate to ask whether it has any value beyond the pedagogical. We find that it has both computational and interpretational value. In a subsequent paper we shall describe the computation of the process $\gamma^*+\gamma^* \to$ hadrons, a rather more intricate computation than the ones presented here. We find that the diagrammatic method provides a more straightforward and transparent calculational tool than the operator-product and renormalization-group machinery, although that may be a matter of personal taste.

As for the interpretational value of the method, it is clear that it enables one to justify with precision the Altarelli-Parisi[2] bremsstrahlung scheme for calculating the anomalous dimensions, including an understanding of the importance of wave-function renormalization in regulating the divergent moments of the bremsstrahlung distributions. More generally, it allows one to make contact with the pictorial parton-model approach. We have demonstrated that the leading-log series (in the axial gauge) arises entirely from the two-particle-reducible ladder graphs, in a given quark channel, in which each rung of the ladder is renormalized one-particle exchange and in which the ladder series factorizes from the simplest renormalized "Born" diagrams used for attachment to the deep-inelastic currents, $\mu^+\mu^-$ pair, high-p_T subprocesses, or other short-distance probe. Thus all parton-model applications are in fact justified in the leading-log approximation, provided that: (a) the quark-parton distributions incorporate the scale breaking as calculated from the leading-log or asymptotic freedom approaches, or are those directly measured at appropriate Q^2 values in deep-inelastic scattering, and (b) that the elementary short-distance subprocess is expressed in terms of fully renormalized coupling constants e_R^2 or $\alpha_s(Q^2)$, the extra $(\ln Q^2)^{-\gamma_F(\gamma_G)}$ wave-function renormalization pieces for each initial or final quark (gluon) participating in the subprocess having been incorporated into the scale-broken distribution functions as discussed in Sec. II. We learn that in justifying the leading-log factorization, integration over $k_\perp$ of the quarks is crucial. Thus, for instance, if a $\mu^+\mu^-$ pair of given Q^2 *and* $Q_\perp$ is examined, i.e., the annihilating quark and antiquark have correlated $k_\perp$'s, then the simple parton-model factorized approach is not obviously correct. We also learn, from the diagrammatic structure of terms which do not contribute to leading log but are down by only a single log, that the approach of factorizing a parton distribution

FIG. 14. Examples of graphs contributing in next to leading log for (a) $\mu^+\mu^-$ pair production, (b) deep-inelastic scattering.

from the simplest "Born" (no-loop) contribution to the given short-distance process does not work to next order in $1/\ln Q^2$. For instance, in the μ-pair case a diagram such as Fig. 14(a) will contribute a term of order $1/\ln Q^2$ relative to the leading-log series (in the axial gauge). How to relate this $1/\ln Q^2$ correction to similar ones for deep-inelastic scattering, such as the Fig. 14(b) diagram, is not apparent. However, a general calculation procedure is obvious: One calculates the short distance 2PI (in all channels) component of the cross section to a desired order in $\alpha_s(Q^2)$. This will bring in the 2PI parts of diagrams like 14(a) and 14(b) as higher-order corrections to the simplest "Born" contribution; this 2PI component is then folded together with the full scale-broken distributions of the quarks (or gluons) participating (i.e., entering into) this 2PI component. The scale-broken quark/gluon distribution functions contain all knowledge of the external hadrons and related mass singularities, and theoretically may be computed to any desired order in $1/\ln Q^2$ by systematically retaining higher-order corrections to the 2PI kernel. These higher-order corrections to the scale-broken quark-gluon distribution functions are, however, not directly measured by the deep-inelastic structure function, which is sensitive, as well, to higher-order corrections to the two-particle irreducible-current attachment kernel.

ACKNOWLEDGMENTS

We wish to acknowledge very helpful conversations with S. Brodsky, P. Le Page, C. H. Llewellyn Smith, and especially T. Appelquist, who called to our attention work on which this paper is based.

During the course of preparation of this manuscript a number of closely-related works have come to our attention.[13-19]

One of us (JFG) would like to acknowledge the generous support of the A. P. Sloan Foundation. We would like to acknowledge the support of the 1977 Aspen Institute for Physics where this work was begun. One of us (JFG) wishes to thank the 1978 Seattle Summer Institute for its support during the completion of the manuscript. This work was supported in part by the U.S. Department of Energy.

APPENDIX A

We consider here the example of the single crossed-ladder 2PI kernel relative to the one-particle exchange kernel [Fig. 15(a) vs 15(b) and 15(c)]. We do this in the context of the reversed Bethe-Salpeter equation (2.14). For $k^2 \gg p^2$ we divide the l^2 integral into the region $l^2 > k^2$ and $l^2 < k^2$. (For simplicity we neglect $l\cdot k$, $l\cdot p$, and $p\cdot k$ dependences which can be easily included using the techniques discussed in the text.) For $l^2 < k^2$ the crossed ladder gives

$$\frac{1}{b^2}\int \frac{dl^2 l^4}{k^4 l^4}(\ln l^2)^{-1/2+\gamma/2}(\ln k^2)^{-3/2-\gamma/2} \sim \frac{1}{b^2 k^2}(\ln k^2)^{-2}, \tag{A1}$$

while $l^2 > k^2$ yields

$$\frac{1}{b^2}\int_{k^2}^{\infty} \frac{dl^2 l^4}{l^8}\frac{(\ln k^2)^{2\gamma}}{(\ln l^2)^{2+2\gamma}} \sim \frac{1}{b^2 k^2}(\ln k^2)^{-2}. \tag{A2}$$

Both regions are suppressed by a full power of $(\ln k^2)^{-1}$ relative to the single-particle exchange graph. In general, the k^2 to ∞ region is obviously unable to yield a leading behavior because the integral is convergent for any 2PI kernel. The $l^2 < k^2$ loop integration region could have become important had the l^2 integration been primitively log divergent as, for instance (neglecting moving coupling constants),

$$\int^{k^2} \frac{dl^2}{l^2} \sim \ln k^2 \tag{A3}$$

instead of

$$\int^{k^2} \frac{dl^2}{k^2} \sim 1. \tag{A4}$$

This same log-divergent integral is that which would be associated with an infrared divergence as $p^2 \to 0$ coming from the lower limit. This is a specific example of the relation between a leading-log derivation and the infrared finiteness of the

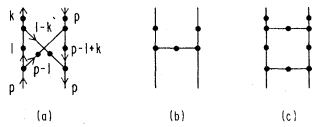

FIG. 15. (a) A crossed ladder two-particle irreducible kernel; (b) the simplest one-particle exchange 2PI kernel; (c) the uncrossed ladder of same order in g^2 as (a).

2PI kernel. The two are equivalent in the $(\phi^3)_6$ and QCD cases. In a general 2PI graph one contracts those lines carrying k (a possibly important region of loop variables is $l^2<k^2$) and examines the reduced graph for log divergences $\int dl^2/l^2$ in the subintegrations. One can show in general that there are none following counting procedures like those discussed in Appelquist and Poggio's Appendix A.[1]

We may also easily compare the crossed-ladder contribution to the ladder contribution [Fig. 15(c)] which yields

$$\frac{1}{bk^2\ln k^2}\int^{k^2}\frac{dl^2l^4}{l^6b\ln l^2}+\frac{(\ln k^2)^{2\gamma}}{b^2}\int_{k^2}^{\infty}\frac{dl^2l^4}{l^8}\frac{1}{(\ln l^2)^{2+2\gamma}}\sim\frac{1}{k^2b^2\ln k^2}\left(\ln\ln k^2+\frac{1}{\ln k^2}\right). \tag{A5}$$

We see that the ladder contribution begins to develop an exponential series $1/\ln k^2(1+\ln\ln k^2+\frac{1}{2}(\ln\ln k^2)^2+\ldots)$ from the $l^2<k^2$ region. The $l^2>k^2$ region is suppressed by a full $(\ln k^2)^{-1}$.

APPENDIX B

In this appendix we show in detail some sample calculations in our formalism, and list the results for the anomalous dimensions. First consider the contribution of the $q\bar{q}\to gg$ ladder kernel to the $gg\to\gamma^*\gamma^*$ amplitude, G_1, Fig. 16(a) (including a factor of -2 for summing over closed quark and antiquark loops)

$$G^1_{\sigma\tau}=-2\int\frac{d^4k}{(2\pi)^4}\frac{\mathrm{Tr}[\not k\gamma_\tau(\not k-\not p)\gamma_\sigma\not k F_1]}{k^4(k-p)^2b\ln k^2}(\ln k^2)^{\vec\gamma_F-\vec\gamma_G}. \tag{B1}$$

We wish to isolate the $g_{\sigma\tau}$ part of this amplitude. We can do this by noting that the polarization sum operator

$$P_{\sigma\tau}(p)=-g_{\sigma\tau}+\frac{p_\sigma q_\tau+p_\tau q_\sigma}{p\cdot q}-\frac{q^2p_\sigma p_\tau}{(p\cdot q)^2} \tag{B2}$$

effectively projects out the $g_{\sigma\tau}$ part of the amplitude since other terms are small or zero. For instance, any term proportional to q_σ or q_τ yields zero in the Lipatov gauge, while any term proportional to p_σ or p_τ yields an order p^2/q^2 contribution relative to

$$P_{\sigma\tau}g_{\sigma\tau}=-4+2+O(p^2/q^2)\sim-2. \tag{B3}$$

Thus [see Eq. (3.7b)]

$$P_{\sigma\tau}G^1_{\sigma\tau}=-2\nu\sum_{n=0}^{\infty}g_{1,n}(p^2,q^2)\omega^{n-1}/q^2 \tag{B4}$$

receives a contribution from Eq. (B1) of the form

$$I=-2\int\frac{d^4k(\ln k^2)^{\vec\gamma_F-\vec\gamma_G}}{(2\pi)^4k^4b\ln k^2}\sum_{m=0}^{\infty}\left(\frac{2k\cdot p}{k^2}\right)^m P_{\sigma\tau}\,\mathrm{Tr}[\not k\gamma_\tau(\not k-\not p)\gamma_\sigma\not k\not q]\sum_{n=0}^{\infty}f_{1,n}(k^2,q^2)\left(\frac{2q\cdot k}{q^2}\right)^{n-1}\frac{1}{q^2}, \tag{B5}$$

where we have dropped quark label and color subscripts.

In evaluating $P_{\sigma\tau}\,\mathrm{Tr}[\ ]$ we drop terms which do not contribute in leading log and obtain

$$P_{\sigma\tau}\,\mathrm{Tr}[\not k\gamma_\sigma(\not k-\not p)\gamma_\tau\not k\not q]=8p\cdot qk^2+16\frac{q\cdot k}{p\cdot q}(2p\cdot kq\cdot k-k^2p\cdot q)+0. \tag{B6}$$

We now use the angular integration identity (for the leading-log terms)

$$\int\frac{d\Omega_k}{(2\pi)^4}\left(\frac{2k\cdot p}{k^2}\right)^m\left(\frac{2k\cdot q}{q^2}\right)^j=\delta_{mj}\frac{1}{8\pi^2(m+1)}\left(\frac{2p\cdot q}{q^2}\right)^m \tag{B7}$$

to obtain (including an extra minus sign to convert the integration to Euclidean metric, and with $\nu=p\cdot q$)

$$I=\frac{-16\nu}{q^2}\int^{q^2}\left(-\frac{1}{2}\frac{dk^2}{k^2}\right)\frac{(\ln k^2)^{-1+\vec\gamma_F-\vec\gamma_G}}{8\pi^2b}\sum_{n=0}^{\infty}f_{1,n}(k^2,q^2)\left[\frac{1}{n}+\left(\frac{2}{n+2}-\frac{2}{n+1}\right)\right]\left(\frac{2p\cdot q}{q^2}\right)^{n-1}. \tag{B8}$$

So we have a piece in our dk^2 integral equation for $g_{1,n}$ of the form

$$g_{1,n}(p^2,q^2)=\frac{-8}{16\pi^2}\int^{q^2}\frac{dk^2(\ln k^2)^{\vec\gamma_F-\vec\gamma_G}}{k^2b\ln k^2}\left(\frac{n^2+n+2}{n(n+1)(n+2)}\right)f_{1,n}(k^2,q^2). \tag{B9}$$

Comparing this result with Eq. (3.9b) we see that

$$b^n_{GF}=\frac{-4}{8\pi^2}\frac{n^2+n+2}{n(n+1)(n+2)}. \tag{B10}$$

As an example of the leading-log approximations built into (B5) we show in what sense the third term of $P_{\sigma\tau}\,\mathrm{Tr}[\ ]$ in (B6) is 0. In actual fact it is

$$-\frac{q^2}{(p\cdot q)^2}\mathrm{Tr}[\not k\not p(\not k-\not p)\not p\not k\not q]\overset{p^2\,\mathrm{small}}{\approx}-\frac{q^2}{(p\cdot q)^2}\mathrm{Tr}(\not k\not p\not k\not p\not k\not q)=-\frac{8p\cdot kq^2}{(p\cdot q)^2}(2q\cdot kp\cdot k-\nu k^2). \tag{B11}$$

Since $p\cdot k$ is effectively of order k^2, this term is of order k^4 and cannot yield log-divergent integrals.

As a second example we consider the calculation of b_{FF} and $\bar\gamma_F$ for W_1. As is well known, these are separately gauge- and regularization-scheme-dependent quantities. Only the combination associated with the anomalous dimension of the gauge-invariant quantity W_1 is invariant. The graph we are considering is shown in Fig. 17 which yields a contribution to the behavior of F_1 of the form

$$F_1=\int\frac{d^4k}{(2\pi)^4}\frac{(\gamma_\alpha\not kF_1\not k\gamma_\beta)P_{\beta\alpha}(k-p)}{b\ln k^2(k-p)^2}. \tag{B12}$$

Consider first the $-g_{\alpha\beta}$ part of $P_{\alpha\beta}$.

$$\gamma_\alpha\not kF_1\not k\gamma_\beta(-g_{\alpha\beta})=\frac{1}{q^2}\sum_{n=0}^{\infty}f_{1,n}(k^2,q^2)\left(\frac{2q\cdot k}{q^2}\right)^{n-1}\left(\frac{-2}{q^2}\right)(k^2\not k-2q\cdot k\not k+k^2\not q). \tag{B13}$$

As usual, only the second two terms survive in the leading-log approximation. Using (B7) and the leading-log identity

$$\int\frac{d\Omega_k}{(2\pi)^4}\left(\frac{2p\cdot k}{k^2}\right)^n\left(\frac{2q\cdot k}{q^2}\right)^m\not k\sim\frac{\not qk^2}{q^2}\frac{\delta_{m,n+1}}{8\pi^2(n+2)}\left(\frac{2p\cdot q}{q^2}\right)^n, \tag{B14}$$

we obtain, after expanding $(k-p)^{-2}$ and incorporating the minus sign for conversion to a Euclidean integral

$$\not q\sum_{n=0}^{\infty}\frac{1}{q^2}f_{1,n}(p^2,q^2)\left(\frac{2p\cdot q}{q^2}\right)^{n-1}=\frac{\not q}{q^2}\int\frac{1}{2}\frac{dk^2}{k^2b\ln k^2}\frac{2}{8\pi^2}\sum_n\left(\frac{1}{n}-\frac{1}{n+1}\right)\left(\frac{2p\cdot q}{q^2}\right)^{n-1}. \tag{B15}$$

That is, there is a term in the integral equation (3.9a) of the form

$$f_{1,n}(p^2,q^2)=\frac{b^n_{FF}}{b}\int\frac{dk^2}{k^2\ln k^2}f_{1,n}(k^2,q^2) \tag{B16}$$

with

$$b^n_{FF}=\frac{1}{8\pi^2n(n+1)}.$$

The other terms in $P_{\alpha\beta}$ also yield contributions to b^n_{FF}; namely,

$$b^n_{FF}=\frac{1}{8\pi^2}\begin{cases}\dfrac{1}{n(n+1)} & \text{(a)}\\[2mm] -2\displaystyle\sum_{m=1}^{n}\frac{1}{m} & \text{(b)}\\[2mm] 0. & \text{(c)}.\end{cases} \tag{B17}$$

The last two terms depend explicitly on our method of handling the singularity at $(k-p)\cdot q=0$. For instance, the only contributing integration for the $[(k-p)\cdot q]^{-2}$ propagator term in the KKS regularization scheme reduces to the form

FIG. 16. The $gg\to q\bar q$ ladder kernel contribution to $gg\to\gamma^*\gamma^*$, i.e., to G of Eq. (3.7). (b) The $q\bar q\to gg$ ladder contribution to $q\bar q\to\gamma^*\gamma^*$, i.e., to F of Eq. (3.7).

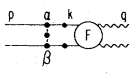

FIG. 17. Contribution to F_1 from the $q\bar q\to q\bar q$ ladder kernel, Eq. (B12).

$$\int \frac{d^4k}{(2\pi)^4 k^2 (q\cdot k)^2} = -\frac{2}{q^2}\int \frac{d^4k}{(2\pi)^4 k^4}. \tag{B18}$$

One must of course calculate γ_F using the same gluon propagator and regularization scheme. One obtains

$$\bar{\gamma}_F = -\frac{3}{2}\frac{1}{8\pi^2 b}. \tag{B19}$$

The net power of $\ln q^2$ arising from those various components as per Eqs. (3.10) and (3.11) is

$$f_n(p^2, q^2) \sim (\ln q^2)^{a_n} \tag{B20}$$

with

$$a_n = \frac{b^n_{FF}}{b} - \bar{\gamma}_F = -\frac{1}{16\pi^2 b}\left(1 - \frac{2}{n(n+1)} + 4\sum_{m=2}^{n}\frac{1}{m}\right), \tag{B21}$$

which is the standard result for the anomalous dimension of the nonsinglet component of W_1.

In the preceding, of course, we have not written explicitly the group-theoretical coefficients $C_2(R) = \frac{4}{3}$ for b_{FF} and γ_F and $T(R) = \frac{1}{2}$, per fermion type, for b_{GF}. [Our convention is the standard one: $\mathrm{Tr}(\lambda_a{}^2) = 2$ and $L_I = g\bar{\psi}(\lambda_a/2)\gamma_\mu \psi A^{\mu a}$].

We conclude this Appendix by listing the values of the γ's and b's in our gauge and regularization scheme:

$$\begin{aligned}
\gamma_F &= -\frac{3}{2}\frac{1}{8\pi^2}\left(\frac{4}{3}\right),\\
\gamma_G &= -\frac{1}{16\pi^2}\left[\frac{11}{3}(3) - \frac{4}{3}\left(\frac{1}{2}\right)n_f\right],\\
b^n_{FF} &= -\frac{1}{16\pi^2}\left(-\frac{2}{n(n+1)} + 4\sum_{m=1}^{n}\frac{1}{m}\right)\left(\frac{4}{3}\right),\\
b^n_{GF} &= \frac{-4}{8\pi^2}\frac{n^2+n+2}{n(n+1)(n+2)}\left(\frac{1}{2}\right),\\
b^n_{FG} &= -\frac{1}{16\pi^2}\frac{n^2+n+2}{n(n^2-1)}\left(\frac{4}{3}\right),\\
b^n_{GG} &= -\frac{2}{8\pi^2}\left(-\frac{1}{n(n-1)} - \frac{1}{(n+1)(n+2)} + \sum_{m=1}^{n}\frac{1}{m}\right)(3).
\end{aligned} \tag{B22}$$

The numbers in ( ) are the group-theoretical numbers $C_2(G) = 3$, $C_2(R) = \frac{4}{3}$, and $T(R) = \frac{1}{2}$ (per fermion type), n_f is the number of fermion flavors. The normalizations and signs of F_1 and G_1 have been chosen so that these results can be directly compared with those of Gerogi and Politzer and of Gross and Wilczek.[4] One curious feature of the Lipatov gauge and the KKS regularizations scheme is that b^n_{FF} and $\bar{\gamma}_F$ both differ from those calculated, say, in Feynman gauge. Of course only the amplitude W_1 is gauge invariant, and there these quantities appear in the standard anomalous dimension combination

$$\frac{b^n_{FF}}{b} - \bar{\gamma}_F = -\frac{1}{16\pi^2 b}\left(1 - \frac{1}{n(n+1)} + 4\sum_{m=2}^{n}\frac{1}{m}\right)\left(\frac{4}{3}\right) \tag{B23}$$

as discussed above. The above is the standard result. One sees this gauge dependence of b_{FF} and $\bar{\gamma}_F$ in a much more severe fashion in our justification of the Altarelli-Parisi scheme in Sec. IV. Each is separately infinite, when calculated naively using light-cone techniques, but the combination again yields the usual answer.

APPENDIX C

In this Appendix we discuss the solution to (3.9a) and (3.9b) for the singlet case; the index $\alpha = 1$ for W_1 is understood. The number of flavors is n_f. We define the singlet quantities

$$\sum_{i=1}^{n_f} f_n^i \equiv f_n$$

and

$$\sum_{i=1}^{n_f} F_n^i \equiv F_n = 2\sum_{i=1}^{n_f} Q_i{}^2.$$

The Eqs. (3.9) take the form when summed over i,

$$f_n(p^2, q^2) = F_n(\ln q^2)^{-\bar{\gamma}_F} + \frac{b^n_{FF}}{b}\int_{p^2}^{q^2}\frac{dk^2}{k^2}(\ln k^2)^{-1} f_n(k^2, q^2) + \frac{b^n_{FG}}{b}\int_{p^2}^{q^2}\frac{dk^2}{k^2}(\ln k^2)^{-1+\bar{\gamma}_G-\bar{\gamma}_F} n_f g_n(k^2, q^2), \tag{C1a}$$

$$n_f g_n(p^2, q^2) = 0 + n_f\frac{b^n_{GF}}{b}\int_{p^2}^{q^2}\frac{dk^2}{k^2}(\ln k^2)^{-1+\bar{\gamma}_F-\bar{\gamma}_G} f_n(k^2, q^2) + \frac{b^n_{GG}}{b}\int_{p^2}^{q^2}\frac{dk^2}{k^2}(\ln k^2)^{-1} n_f g_n(k^2, q^2). \tag{C1b}$$

Define

$$\begin{aligned}
\gamma^n_{11} &= \bar{\gamma}_F - \frac{b^n_{FF}}{b}, \quad \gamma^n_{12} = -\frac{b_{FG}}{b},\\
\gamma^n_{21} &= -\frac{b^n_{GF}}{b}n_f, \quad \gamma_{22} = \bar{\gamma}_G - \frac{b^n_{GG}}{b}.
\end{aligned} \tag{C2}$$

We now temporarily drop the n superscripts and subscripts. It is easily verified that the forms

$$f(p^2, q^2) = \left[C_{11}\left(\frac{\ln p^2}{\ln q^2}\right)^{\gamma_1} + C_{12}\left(\frac{\ln p^2}{\ln q^2}\right)^{\gamma_2}\right](\ln p^2)^{-\bar{\gamma}_F} \tag{C3a}$$

and

$$n_f g(p^2, q^2) = \left[C_{21} \left(\frac{\ln p^2}{\ln q^2} \right)^{\gamma_1} + C_{22} \left(\frac{\ln p^2}{\ln q^2} \right)^{\gamma_2} \right] (\ln p^2)^{-\bar{\gamma}_G} \tag{C3b}$$

satisfy (C1a) and (C1b) provided

$$C_{11} + C_{12} = F, \quad C_{21} + C_{22} = 0, \tag{C4}$$

and

$$\begin{aligned} \gamma_1 - \gamma_{11} &= \gamma_{12} C_{21} / C_{11}, \\ \gamma_2 - \gamma_{11} &= \gamma_{12} C_{22} / C_{12}, \\ \gamma_1 - \gamma_{22} &= \gamma_{21} C_{11} / C_{21}, \\ \gamma_2 - \gamma_{22} &= \gamma_{21} C_{12} / C_{22}. \end{aligned} \tag{C5}$$

The latter imply the eigenvalue condition

$$2\gamma_{1,2} = \gamma_{11} + \gamma_{22} \mp [(\gamma_{11} - \gamma_{22})^2 + 4\gamma_{12}\gamma_{21}]^{1/2}. \tag{C6}$$

We may of course solve (C4), (C5), and (C6) for the explicit values of C_{11}, C_{12}, C_{21}, and C_{22}. Defining

$$\delta = [(\gamma_{11} - \gamma_{22})^2 + 4\gamma_{12}\gamma_{21}]^{1/2} \tag{C7}$$

and

$$r \equiv \frac{(\gamma_2 - \gamma_{11})(\gamma_1 - \gamma_{22})}{\gamma_{12}\gamma_{21}} = \frac{\gamma_{11} - \gamma_{22} - \delta}{\gamma_{11} - \gamma_{22} + \delta}, \tag{C8}$$

we obtain

$$\begin{aligned} C_{11} &= \frac{Fr}{r-1} = F\left(\frac{\gamma_{11} - \gamma_{22} - \delta}{-2\delta} \right), \\ C_{12} &= F - C_{11} = F\left(\frac{\gamma_{22} - \gamma_{11} - \delta}{-2\delta} \right), \\ -C_{21} &= C_{22} = \frac{F\gamma_{21}}{\delta}. \end{aligned} \tag{C9}$$

Had there been a Born term for $n_f g$ (as occurs in W_L) call it G, we would have obtained

$$C_{11} + C_{12} = F, \quad C_{21} + C_{22} = G, \tag{C4'}$$

with the consequence

$$\begin{aligned} C_{11} &= F\left(\frac{\gamma_{11} - \gamma_{22} - \delta}{-2\delta} \right) - G\frac{\gamma_{12}}{\delta}, \\ C_{12} &= F\left(\frac{\gamma_{22} - \gamma_{11} - \delta}{-2\delta} \right) + G\frac{\gamma_{12}}{\delta}, \\ C_{21} &= -F\frac{\gamma_{21}}{\delta} + G\left(\frac{\gamma_{22} - \gamma_{11} - \delta}{-2\delta} \right), \\ C_{22} &= F\frac{\gamma_{21}}{\delta} + G\left(\frac{\gamma_{11} - \gamma_{22} - \delta}{-2\delta} \right). \end{aligned} \tag{C5'}$$

Finally, we wish to record an identity which will be useful in the context of two-photon deep-inelastic physics. Using $\gamma_2 + (\gamma_2 - \gamma_1)/(r-1) = \gamma_{22}$ it is easy to establish that

$$\frac{C_{11}}{1+\gamma_1} + \frac{C_{12}}{1+\gamma_2} = \frac{1}{d}[F(1+\gamma_{22}) + G\gamma_{12}], \tag{C10}$$

where

$$\begin{aligned} d &= (1+\gamma_1)(1+\gamma_2) \\ &= 1 + \gamma_{11} + \gamma_{22} + \gamma_{11}\gamma_{22} - \gamma_{12}\gamma_{21}. \end{aligned} \tag{C11}$$

APPENDIX D

In this appendix we show why the leading logarithm must be lost in the top loop of the ladder in the calculation of W_L. For simplicity we use the $(\phi^3)_6$ notation of Sec. II. At the simplest level we can compare two two-loop calculations; one in which the leading log is lost in the top ladder loop to one in which it is lost in the second loop [Figs. 18(a) vs 18(b)]. The structure of a leading-log contribution is

$$\gamma^2 \int_{p^2}^{q^2} \frac{dl^2}{l^2} \frac{1}{\ln l^2} \int_{l^2}^{q^2} \frac{dk^2}{k^2 \ln k^2} = \frac{\gamma^2}{2} \left[\ln\left(\frac{\ln q^2}{\ln p^2} \right) \right]^2, \tag{D1}$$

where γ is the regular integral result at each loop. The inverse logarithms, of course, come from the moving coupling constant. Loss of the leading log at the top loop corresponds to the structure

$$\gamma^2 \int_{p^2}^{q^2} \frac{dl^2}{l^2} \frac{1}{\ln l^2} \int_{l^2}^{q^2} \frac{dk^2}{k^2} \left(\frac{k^2}{q^2} \right) \frac{1}{\ln k^2} \sim \frac{\gamma^2}{\ln q^2} \ln\left(\frac{\ln q^2}{\ln p^2} \right), \tag{D2}$$

while loss of the leading-log at the second loop corresponds to the structure

$$\begin{aligned} \gamma^2 \int_{p^2}^{q^2} \frac{dl^2}{l^2} \left(\frac{l^2}{q^2} \right) \frac{1}{\ln l^2} \int_{l^2}^{q^2} \frac{dk^2}{k^2 \ln k^2} &= \gamma^2 \int_{p^2}^{q^2} \frac{dl^2}{q^2 \ln l^2} \ln\left(\frac{\ln q^2}{\ln l^2} \right) \\ &= \gamma^2 (\ln q^2)^{-2} + O((\ln q^2)^{-3}). \end{aligned} \tag{D3}$$

In general, in an n-loop graph, if we lose the leading log at the mth loop from the top, the structure is

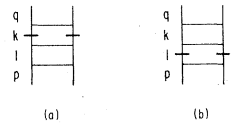

FIG. 18. (a) Loss of a leading log (indicated by - marks) in the top loop of a two-loop ladder compared to (b) loss of the leading log in the second loop.

$$\frac{\gamma^n}{(m-1)!}\int_{p^2}^{q^2}\frac{dk_n^2}{k_n^2\ln k_n^2}\int_{k_n^2}^{q^2}\frac{dk_{n-1}^2}{k_{n-1}^2\ln k_{n-1}^2}\cdots\int_{k_{m+1}^2}^{q^2}\frac{dk_m^2}{q^2\ln k_m^2}\left[\ln\left(\frac{\ln q^2}{\ln k_m^2}\right)\right]^{m-1}$$

$$\sim\gamma^n\int_{p^2}^{q^2}\frac{dk_n^2}{k_n^2\ln k_n^2}\cdots\int_{k_{m+2}^2}^{q^2}\frac{dk_{m+1}^2}{k_{m+1}^2\ln k_{m+1}^2}(\ln q^2)^{-m}$$

$$\sim\gamma^n(\ln q^2)^{-m}\left[\ln\left(\frac{\ln q^2}{\ln p^2}\right)\right]^{n-m}. \tag{D4}$$

Here we have used the identity

$$\frac{1}{q^2}\int_{p^2}^{q^2}dk^2(\ln k^2)^{-n}\ln^m\left(\frac{\ln q^2}{\ln k^2}\right)\sim m!\,(\ln q^2)^{-n-m}, \tag{D5}$$

derived by differentiating m times with respect to λ and setting $\lambda=0$ in the identity

$$\frac{1}{q^2}\int_{p^2}^{q^2}dk^2(\ln k^2)^{-n}\left(\frac{\ln q^2}{\ln k^2}\right)^{\lambda}\sim(\ln q^2)^{-n}\left[1+\frac{n+\lambda}{\ln q^2}+\frac{(n+\lambda)(n+\lambda+1)}{(\ln q^2)^2}+\cdots\right]+O(p^2/q^2). \tag{D6}$$

[The series (D6) is easily derived by repeated integration by parts.] Taking $\sum_{n=m}^{\infty}$ of (D4) we find that loss of the leading log at the mth loop results in a net ladder sum of order

$$\left(\frac{\ln q^2}{\ln p^2}\right)^{\gamma}\frac{\gamma^m}{(\ln q^2)^m}. \tag{D7}$$

Obviously the $m=1$ term dominates.

One important point should be noticed; the loss of the leading log is characterized by a k^2/q^2 correction. This is because we must generate a structure [for instance, $q\!\!\!/(q\cdot\Delta)^2$ of (3.19a)] which is explicitly of order q^2/k^2 relative to the Dirac structure which is naturally present in the leading-log pieces of the mth loop.

APPENDIX E

In this appendix we first calculate γ_F using the infinite-momentum, light-cone techniques, and conclude with the calculation of b^n_{FG} and b^n_{GF}. By the Ward identity we may calculate the wave-function normalization behavior from the vertex diagram of Fig. 19. For the spin average, at zero momentum transfer, we have

$$\tfrac{1}{2}\mathrm{Tr}(\gamma_0 p\!\!\!/)F_1(0)=2p_0F_1(0)$$

$$=\int'\frac{d^4k}{(2\pi)^4}\frac{P_{\alpha\beta}(p-k)}{(p-k)^2k^4}\times\tfrac{1}{2}\mathrm{Tr}(\gamma_0 k\!\!\!/\gamma_\alpha p\!\!\!/\gamma_\beta k\!\!\!/). \tag{E1}$$

The d^4k integration will be performed using the light-cone techniques of Eq. (4.6).

As before there are three contributions corresponding to the three components of $P_{\alpha\beta}$. We wish to find the terms which yield an integration of the form $\int dk_\perp^2/k_\perp^2$. These terms are independent of $q_\perp$ and ν. This must be true since we know that terms which depend on $q_\perp$ or ν, through the axial gauge used for $P_{\alpha\beta}(p-k)$, must cancel because $F_1(0)$ has no knowledge of $q_\perp$ or ν. Thus, for example, structures such as

$$\int\frac{dk_\perp^2}{k_\perp^2}\frac{k_\perp^2}{\nu}$$

must cancel among themselves. We obtain

$$\tfrac{1}{2}\mathrm{Tr}(\gamma_0 k\!\!\!/\gamma_\alpha p\!\!\!/\gamma_\beta k\!\!\!/)P_{\alpha\beta}(p-k)\sim 2p_0k^2\times\begin{cases}2z-2 & \text{(a)}\\ -\dfrac{4z}{1-z} & \text{(b)}\\ 0, & \text{(c)}\end{cases} \tag{E2}$$

where we have labeled the $-g_{\alpha\beta}$, etc., parts of $P_{\alpha\beta}$ by (a), (b), and (c) as before. The sum of the contributions listed in (E2) yields the results [recall that $k^2\sim-k_\perp^2/(1-z)$ etc.]

$$F_1(0)=\int_0^1 dz\int^{\Lambda^2}\frac{dk_\perp^2}{8\pi^2k_\perp^2}\frac{1+z^2}{1-z}$$

$$=\ln\Lambda^2\frac{1}{8\pi^2}\int dz\,\frac{1+z^2}{1-z}. \tag{E3}$$

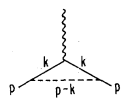

FIG. 19. The vertex diagram used to calculate the lowest-order contribution to $Z_1=Z_2$.

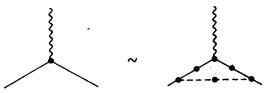

FIG. 20. The self-consistent integral equation which must be obeyed by the $\gamma q\bar{q}$ vertex and fermion propagator.

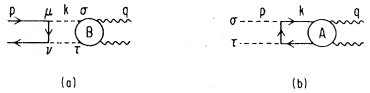

FIG. 21. (a) The $q\bar{q}\to gg$ ladder contribution to $A(q\bar{q}\to\gamma^*\gamma^*)$. (b) The $gg\to q\bar{q}$ ladder contribution to $B(gg\to\gamma^*\gamma^*)$.

In standard fashion γ_F is read off as the coefficient of $\ln\Lambda^2$ in this lowest-order calculation and $\bar{\gamma}_F=\gamma_F/b$. Note that the fermion propagator or, equivalently (by the Ward identity) the inverse of the photon $q\bar{q}$ vertex behavior,

$$S_F(p)\sim\frac{\not p}{p^2}(\ln p^2)^{\bar{\gamma}_F} \tag{E4}$$

actually is the self-consistent solution of the integral equation diagrammed in Fig. 20. The bare vertex Born term is absent asymptotically since the $\gamma q\bar{q}$ vertex behavior, $(\ln p^2)^{-\bar{\gamma}_F}$, is such that the power $-\bar{\gamma}_F$ (once regularized) is positive.

We now turn to calculations of b^n_{FG} and b^n_{GF}. They are defined as the distribution function moments which connect the spin-average amplitude $b'(p^2,q^2,2p\cdot q)=2p\cdot qb$ of Eq. (4.11) and the gluon amplitude $2c'(p^2,q^2,2p\cdot q)=2p\cdot qc$, where b and c are defined by the fermion and gluon-amplitude leading terms, analogous to (3.7),

$$A(q\bar{q}\to\gamma^*\gamma^*)\sim\not q\, b(p^2,q^2,2p\cdot q),$$
$$B_{\alpha\beta}(g_\alpha g_\beta\to\gamma^*\gamma^*)\sim g_{\alpha\beta}p\cdot q\, c(p^2,q^2,2p\cdot q)\ , \tag{E5}$$

and we have temporarily dropped color indices.

We calculate the diagrams of Figs. 21(a) and 21(b). For Fig. 21(a) the illustrated contribution to the spin-average amplitude

$$\tfrac{1}{2}\mathrm{Tr}(\not p b\not q)=2p\cdot qb=b'$$

is obtained from the trace structure

$$\text{“Tr”}=\tfrac{1}{2}\mathrm{Tr}[\not p\gamma_\nu(\not p-\not k)\gamma_\mu]P_{\mu\sigma}(k)P_{\nu\tau}(k)g_{\sigma\tau}$$
$$\times c'(k^2,q^2,2q\cdot k)\ . \tag{E6}$$

One quickly discovers that in the light-cone techniques the only important contributions come from the terms

$$P_{\mu\sigma}(k)P_{\nu\tau}(k)g_{\sigma\tau}\sim g_{\nu\mu}-\frac{k_\mu q_\nu+k_\nu q_\mu}{q\cdot k}+\frac{q_\mu q_\nu k^2}{(q\cdot k)^2}\ , \tag{E7}$$

which combined with the above trace yields asymptotically

$$\text{“Tr”}\sim 4p\circ k\,\frac{1+(1-z)^2}{z^2}\sim 2k^2\,\frac{1+(1-z)^2}{z^2}\ . \tag{E8}$$

Inserted into the integral-equation contribution of Fig. 21(a) this yields

$$b'(p^2,q^2,2p\cdot q)=-\int\frac{dk_\perp^2}{8\pi^2 bk_\perp^2\ln k_\perp^2}\int_x^1\frac{dz}{z}\,\frac{1+(1-z)^2}{z}\,c'(k^2,q^2,2q\cdot k)\ . \tag{E9}$$

The moments $f_{1,n}$ and $q_{1,n}$ (defined earlier) are the moments of b' and $2c'$ (note factor of 2)

$$f_{1,n}(q_\perp^2)=\frac{b^n_{FG}}{b}\int\frac{dk_\perp^2}{k_\perp^2\ln k_\perp^2}\,g_{1,n}(k_\perp^2)\ , \tag{E10}$$

where b^n_{FG} is as given in Eq. (4.22) (which includes the color factor).

The contribution of Fig. 21(b) to $P_{\sigma\tau}(p)[g_{\sigma\tau}c']=-2c'(p^2,q^2,2q\cdot p)$ is obtained from the trace structure

$$(-2)\mathrm{Tr}[\gamma_\sigma\not k\not q\not k\gamma_\tau(\not k-\not p)]P_{\sigma\tau}(p)b(p^2,q^2,2p\cdot q)\sim(-2)b2k\circ q2k^2\,\frac{4z^2-4z+2}{z}\ . \tag{E11}$$

[This is the light-cone reduction of the corresponding trace of Appendix B, (B5). The -2 is the fermion quark+antiquark loop factor.] Thus we have

$$c'(p^2,q^2,2p\circ q)=\int\frac{dk_\perp^2}{bk_\perp^2\ln k_\perp^2}\,\frac{-2}{8\pi^2}\int_x^1\frac{dz}{z}\,[z^2+(1-z)^2]\,b'(k^2,q^2,2q\cdot k)\ . \tag{E12}$$

Hence the moments of $2c'$ and b' are related by

$$g_{1,n}(q_\perp^2)=\frac{b^n_{GF}}{b}\int\frac{dk_\perp^2}{k_\perp^2\ln k_\perp^2}f_{1,n}(k_\perp^2)\,, \tag{E13}$$

with b^n_{GF} as given in (4.22).

APPENDIX F

In this section we outline calculational details of b_{GG} and γ_G. Figure 22 shows the $gg\to gg$ ladder-kernel contribution of importance. We use the light-cone notation. The contribution to $B_{\mu\nu}$ (dropping color indices) is

$$B_{\mu\nu}(p,q)=\int V^{\mu\sigma\alpha}(p,-k,k-p)V^{\nu\beta\tau}(-p,p-k,k)D_{\alpha\beta}(k-p)D_{\sigma\xi}(k)D_{\tau\eta}(k)B_{\xi\eta}(k,q)\frac{d^4k}{(2\pi)^4 b\ln k^2}\,. \tag{F1}$$

Note that we use the fact that the three-gluon renormalized coupling squared has the same asymptotic behavior as the $gq\bar{q}$ renormalized square coupling. It is convenient to take the polarization sum using $P_{\mu\nu}(p)$. The vertices are standard, e.g.,

$$V^{\mu\sigma\tau}(p,-k,k-p)=(p+k)_\alpha g_{\mu\sigma}+(p-2k)_\mu g_{\alpha\sigma}+(k-2p)_\sigma g_{\mu\alpha}\,. \tag{F2}$$

The calculation is separated into two parts. First, we calculate the quantity

$$\begin{aligned}T_{\sigma\tau}&\equiv P_{\sigma\xi}(k)P_{\tau\eta}(k)g_{\xi\eta}\\&=g_{\sigma\tau}+\frac{k^2q_\sigma q_\tau}{(q\cdot k)^2}+k_\sigma k_\tau\left(\frac{q^2}{(q\cdot k)^2}+\frac{q^4k^2}{(q\cdot k)^4}\right)-(k_\sigma q_\tau+k_\tau q_\sigma)\left(\frac{1}{q\cdot k}+\frac{q^2k^2}{(q\cdot k)^3}\right)\,.\end{aligned} \tag{F3}$$

The object $T_{\sigma\tau}$ obeys some useful identities

$$\left.\begin{aligned}&q_\sigma T_{\sigma\tau}=0\,,\\&k_\sigma k_\tau T_{\sigma\tau}\sim 0,\\&g_{\sigma\tau}T_{\sigma\tau}\sim 2,\\&(p_\tau k_\sigma+p_\sigma k_\tau)T_{\sigma\tau}\sim 0,\\&p_\sigma p_\tau T_{\sigma\tau}\sim\frac{k^2(p\cdot q)^2}{(q\cdot k)^2}-2\nu\frac{p\cdot k}{q\cdot k}\,.\end{aligned}\right\}\ \text{in leading log} \tag{F4}$$

In other words we need only look for $g_{\sigma\tau}$ or $p_\sigma p_\tau$ components of the left-hand side of Fig. 22. Picking out these terms we find

$$\begin{aligned}S_{\sigma\tau}&\equiv P_{\mu\nu}(p)V^{\mu\sigma\alpha}V^{\nu\beta\tau}P_{\alpha\beta}(k-p)\\&\sim g_{\sigma\tau}\left(3k^2+2p\cdot k-\frac{4k^2\nu}{q\cdot(k-p)}-\frac{8p\cdot kq\cdot k}{\nu}\right)\\&\quad+8p_\sigma p_\tau\,.\end{aligned} \tag{F5}$$

Hence [using $k^2\sim 2p\cdot k$ at the $(p-k)^2$ pole]

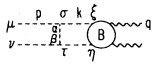

FIG. 22. The $gg\to gg$ ladder contribution to $B(gg\to\gamma^*\gamma^*)$.

$$S_{\sigma\tau}T_{\sigma\tau}=8k^2\left(1-\frac{\nu}{q\cdot(k-p)}-\frac{q\cdot k}{\nu}+\frac{\nu^2}{(q\cdot k)^2}-\frac{\nu}{q\cdot k}\right)\,, \tag{F6a}$$

which in light-cone language becomes

$$\begin{aligned}S_{\sigma\tau}T_{\sigma\tau}&=8k^2\left(1-\frac{1}{z-1}-z+\frac{1}{z^2}-\frac{1}{z}\right)\\&=\frac{8k^2}{z}\left(\frac{z}{1-z}+\frac{1-z}{z}+z(1-z)\right)\,.\end{aligned} \tag{F6b}$$

Of course, in a calculation using the KKS scheme we would simply deal with the (F6a) structure in the manner of Appendix B. In the light-cone method, using $B_{\mu\nu}(p,q)P_{\mu\nu}(p)\sim -2c'(p^2,q^2,2p\cdot q)$ and $B_{\xi\eta}(k,q)\sim g_{\xi\eta}c'(k^2,q^2,2q\cdot k)$, we have

$$\begin{aligned}&2c'(p^2,q^2,2p\cdot q)\\&\quad=\int\frac{dk_\perp^2}{16\pi^2k_\perp^2 b\ln k_\perp^2}\frac{8}{z}\left(\frac{z}{1-z}+\frac{1-z}{z}+z(1-z)\right)\\&\qquad\times c'(k^2,q^2,2q\cdot k)\,,\end{aligned} \tag{F7}$$

which is again of the bremsstrahlung form and yields a relation between $2c'(p,q)$ and $2c'(k,q)$ defined by

$$b^n_{GG} = \frac{2}{8\pi^2}\int_0^1 dz\left(\frac{z}{1-z}+\frac{1-z}{z}+z(1-z)\right)z^{n-1}\,. \tag{F8}$$

The calculation of γ_G follows very similar lines. One uses the Ward identity trick and calculates the diagrams of Figs. 23(a) and 23(b) for the gluon and fermion contributions, respectively. For the gluon part, Fig. 23(a), the γgg coupling is the standard

$$(2k)_\delta g_{\xi\eta} - k_\xi g_{\delta\eta} - k_\eta g_{\delta\xi}\,. \tag{F9}$$

One quickly discovers that only the $g_{\xi\eta}$ piece contributes to the log divergence as in the leading-log ladder derivation, and thus the calculation is very similar to that just performed. For the fermion part, the calculation is essentially the same as that for b_{GF} except for the difference by a factor of 2, which is related to the use of $2c'$ in defining the moments, g_n.

Returning to the gluon part of γ_G, we note that the expression which one naively derives is

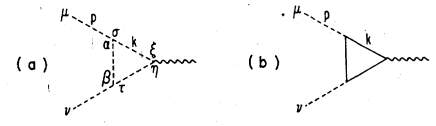

FIG. 23. The gluon (a) and fermion (b) contributions to the vertex (or inverse gluon propagator) renormalization.

$$\gamma_G(\text{gluon}) = \frac{1}{8\pi^2}\int dz\left(\frac{z}{1-z}+\frac{1-z}{z}+z(1-z)\right), \tag{F10}$$

i.e., an integral over the distribution function $G_{gg}(z)$ which has apparent divergences both at $z=0$ and $z=1$. However, because of the symmetry of the integrand it is clear that these divergences are equivalent. We choose to rewrite (F10) in the form given in Eq. (4.23) where all the divergence appears at $z=1$ making cancellation with the $z=1$ divergence in b^n_{GG} apparent.

[1]T. Appelquist and E. Poggio, Phys. Rev. D 10, 3280 (1974).

[2]G. Altarelli and G. Parisi, Nucl. Phys. B126, 298 (1977).

[3]D. Gross and F. Wilczek, Phys. Rev. Lett. 30, 1343 (1973); H. D. Politzer, *ibid.* 30, 1346 (1973).

[4]D. Gross and F. Wilczek, Phys. Rev. D 9, 980 (1974); H. Georgi and H.D. Politzer, *ibid.* 9, 416 (1974).

[5]In QCD this procedure leads to the Nachtmann moments: O. Nachtmann, Nucl. Phys. B63, 237 (1973).

[6]S. D. Drell and T. M. Yan, Phys. Rev. Lett. 25, 316 (1970).

[7]L. N. Lipatov, Yad. Fiz. 20, 181 (1974) [Sov. J. Nucl. Phys. 20, 94 (1975)]; 20, 532 (1974) [20, 287 (1975)]. 20, 532 (1974) [xx, xxx (19xx)].

[8]W. Kainz, W. Kummer, and M. Schweda, Nucl. Phys. B79, 484 (1974).

[9]H. D. Politzer, Phys. Rep. 14C, 129 (1974).

[10]Strictly speaking $F^i_{1,n}$ when calculated is $-2Q_i^2$. This is due to the fact that our momentum, q, exits from the Born term, rather than entering, thus changing the sign of $\not{q}$ and ν from the conventional. At this point we incorporate this trivial sign change.

[11]A. Zee, F. Wilczek, and S. Treiman, Phys. Rev. D 10, 2881 (1974).

[12]See S. Brodsky, F. Close, and J. Gunion, Phys. Rev. D 8, 3679 (1973), Appendix B.

[13]Y. Dokshitser, D. D'Yakanov, and S. Troyan, in Proceedings of the 13th winter school of the Leningrad B. P. Konstantinov Institute of Nuclear Physics, 1978 (SLAC Report No. SLAC-TRANS-183) (unpublished).

[14]R. Ellis, H. Georgi, M. Machacek, H. Politzer, and G. Ross, Phys. Lett. 78B, 281 (1978).

[15]D. Amati, R. Petronzio, and G. Veneziano, Nucl. Phys. B140, 154 (1978); B146, 29 (1978).

[16]Y. Kazama and Y-P. Yao, Phys. Rev. Lett. 41, 611 (1978).

[17]W. J. Stirling, Nucl. Phys. B141, 311 (1978); report DAMPT 78/14 (unpublished) develops some of the correct intuition in these earlier papers.

[18]C. Sachrajda, Phys. Lett. 76B, 100 (1978) proves factorization of scale breaking to first order in α_S.

[19]C. H. Llewellyn Smith, lectures presented at the XVIIth Internationale Universitätswochen für Kernphysik, Schladming, 1978 (unpublished).